

**RESEARCH ARTICLE**

# NF- $\kappa$ B controls axonal regeneration and degeneration through cell-specific balance of RelA and p50 in the adult CNS

Ronny Haenold<sup>1,\*</sup>, Falk Weih<sup>1</sup>, Karl-Heinz Herrmann<sup>2</sup>, Karl-Friedrich Schmidt<sup>3,‡</sup>, Katja Krempler<sup>4</sup>, Christian Engelmann<sup>1</sup>, Klaus-Armin Nave<sup>5</sup>, Jürgen R. Reichenbach<sup>2</sup>, Sigrid Löwel<sup>3,‡</sup>, Otto W. Witte<sup>4</sup> and Alexandra Kretz<sup>4</sup>

**ABSTRACT**

NF- $\kappa$ B is dually involved in neurogenesis and brain pathology. Here, we addressed its role in adult axonogenesis by generating mutations of RelA (p65) and p50 (also known as NFKB1) heterodimers of canonical NF- $\kappa$ B. In addition to RelA activation in astrocytes, optic nerve axonotmesis caused a hitherto unrecognized induction of RelA in growth-inhibitory oligodendrocytes. Intraretinally, RelA was induced in severed retinal ganglion cells and was also expressed in bystander Müller glia. Cell-type-specific deletion of transactivating RelA in neurons and/or macroglia stimulated axonal regeneration in a distinct and synergistic pattern. By contrast, deletion of the p50 suppressor subunit promoted spontaneous and post-injury Wallerian degeneration. Growth effects mediated by RelA deletion paralleled a downregulation of growth-inhibitory Cdh1 (officially known as FZR1) and upregulation of the endogenous Cdh1 suppressor EMI1 (officially known as FBXO5). Pro-degenerative loss of p50, however, stabilized retinal Cdh1. *In vitro*, RelA deletion elicited opposing pro-regenerative shifts in active nuclear and inactive cytoplasmic moieties of Cdh1 and Id2. The involvement of NF- $\kappa$ B and cell-cycle regulators such as Cdh1 in regenerative processes of non-replicative neurons suggests novel mechanisms by which molecular reprogramming might be executed to stimulate adult axonogenesis and treat central nervous system (CNS) axonopathies.

**KEY WORDS:** Anaphase-promoting complex, Axonal regeneration, Cdh1, Manganese-enhanced MRI, NF- $\kappa$ B, p50, RelA, p65, Wallerian degeneration

**INTRODUCTION**

The transcription factor nuclear factor- $\kappa$ B (NF- $\kappa$ B) is ubiquitously expressed and is crucial for various neuropathologies (Kaltschmidt and Kaltschmidt, 2009). In the nervous system, its role is

determined by subunit- and cell-type-specific activation and post-translational modifications of the RelA and p50 (encoded by NFKB1) subunits. Moreover, tissue maturation, its activation in peripheral versus central nervous system (PNS versus CNS) and the context of injury influence cellular NF- $\kappa$ B functions. Studies on neonatal sympathetic and sensory neurons have indicated that the NF- $\kappa$ B family members RelA and p50 can either promote or inhibit axogenesis during postnatal development (Gutierrez and Davies, 2011; Gutierrez et al., 2008). Overexpression of a dominant-negative form of the NF- $\kappa$ B inhibitor I $\kappa$ B $\alpha$  (also known as NFKBIA) in astrocytes indeed limits loco-regional damage after spinal cord injury (SCI) and further stimulates axon sprouting and functional recovery (Brambilla et al., 2005; 2009). However, the significance of individual NF- $\kappa$ B subunits, their activation in separate cell types and their impact on axonal regeneration and Wallerian degeneration currently remain undefined. Intriguingly, a putative involvement of NF- $\kappa$ B in the repulsive feature of white matter substances (Chen et al., 2000) and the anti-growth program exerted by oligodendrocytes (ODC) has not yet been investigated. More importantly, stimulus-dependent axo-nuclear transport of NF- $\kappa$ B as demonstrated by fluorescence recovery after photobleaching (FRAP) analysis of cultivated hippocampal neurons using a RelA-GFP reporter (Meffert et al., 2003) might trigger a cell-intrinsic pro-regenerative or anti-regenerative program in axons themselves.

NF- $\kappa$ B-regulated gene expression is mediated by nuclear translocation of either complexes containing transcriptionally active RelA or homodimers of the transcriptionally inactive p50 subunit. Whereas interference with the upstream kinases IKK $\alpha$ , IKK $\beta$  or IKK $\gamma$  (also known as CHUK, IKBKB and IKBKG, respectively) or overexpression of I $\kappa$ B $\alpha$  results in inhibition of any dimer of the classical NF- $\kappa$ B cascade, subunit-specific knockouts shift the balance between the individual moieties activated. Thus, ablation of either RelA or p50 can propagate dual or even opposing effects, as exemplified for post-ischemic infarct volumes in murine stroke models (Inta et al., 2006; Li et al., 2008; Zhang et al., 2005).

In the present study, we modulated the balance between RelA and p50 subunits specifically in neurons and macroglia of mutant mice either using the Cre/LoxP system or by insertion of a pGK-neo cassette, and we investigated cell-type-specific roles of individual NF- $\kappa$ B subunits in adult axonogenesis. We show that selective suppression of RelA induction in neurons and macroglia (*RelA<sup>CNSKO</sup>*) or in oligodendrocytes (*RelA<sup>ODCKO</sup>*) and astrocytes (*RelA<sup>ASTKO</sup>*) alone differentially and synergistically increased axonal regeneration. By contrast, upregulation of NF- $\kappa$ B activity by ubiquitous p50 deficiency prompted Wallerian degeneration. The divergent effects of RelA and p50 on axon integrity were

<sup>1</sup>Leibniz Institute for Age Research – Fritz Lipmann Institute, Beutenbergstrasse 11, 07745 Jena, Germany. <sup>2</sup>Friedrich Schiller University of Jena Medical School, Institute of Diagnostic and Interventional Radiology, Medical Physics Group, Philosophenweg 3, 07743 Jena, Germany. <sup>3</sup>Friedrich Schiller University of Jena, Institute of General Zoology and Animal Physiology, Erbertstrasse 1, 07743 Jena, Germany. <sup>4</sup>Hans Berger Department of Neurology, Jena University Hospital, Erlanger Allee 101, 07747 Jena, Germany. <sup>5</sup>Max Planck Institute for Experimental Medicine, Department of Neurogenetics, Hermann-Rein-Strasse 3, 37075 Göttingen, Germany.

<sup>\*</sup>Present address: Georg August University, Bernstein Focus Neurotechnology (BFNT) and Johann Friedrich Blumenbach Institute for Zoology and Anthropology, Berliner Strasse 28, 37073 Göttingen, Germany.

\*Author for correspondence (rhaenold@fli-leibniz.de)

reflected in a subunit-specific regulation of the ubiquitin E3 ligase adaptor protein Cdh1 (officially known as FZR1), which was suppressed under axoneogenesis and upregulated under Wallerian degeneration. On the subcellular level, RelA-deficient neuronal cultures exhibited an inactivating shift in Cdh1 protein from the nucleus to the cytoplasm and a reciprocal nuclear accumulation of the pro-regenerative Cdh1 substrate Id2 (inhibitor of DNA binding 2). In summary, balanced levels of the NF- $\kappa$ B subunits RelA and p50 and their orchestration with cell cycle regulators, such as Cdh1, might contribute to define the growth potential of injured CNS fiber networks.

## RESULTS

### Development of the visual system is not impaired in *RelA<sup>CNSKO</sup>* and *p50<sup>KO</sup>* mice

Conditional neuroectodermal deletion of RelA was achieved by nestin-Cre-based recombination of homozygous floxed *relA* alleles (*RelA<sup>CNSKO</sup>*). In these *RelA<sup>CNSKO</sup>* mice, robust reduction of RelA protein in the retina and optic nerve was confirmed by

immunoblotting (data not shown). Recently, we have shown that reduced canonical NF- $\kappa$ B activity in the CNS of *RelA<sup>CNSKO</sup>* mice does not result in a compensatory upregulation of alternative NF- $\kappa$ B subunits but is accompanied by a decline in the expression of the NF- $\kappa$ B target gene *I $\kappa$ B $\alpha$*  (Kretz et al., 2013). By using histopathological analysis, we observed a normal layer architecture of transversal hematoxylin and eosin (HE)-stained retina (Fig. 1A) and an obviously unimpaired relationship between retinal ganglion cells (RGC) and Müller glia, as shown in retinal whole-mount preparations labeled for the RGC marker  $\beta$ -III tubulin (TUJ-1) and the Müller glia marker cellular retinaldehyde-binding protein (CRALBP) (Fig. 1B). By using electron microscopy (Fig. 1C) and immunoblotting (not shown), we found that myelin sheath formation and structural myelin basic protein (MBP) content in naïve optic nerves of *RelA<sup>CNSKO</sup>* mice were similar to those of controls. The number of RGCs ( $P=0.88$ ) in the ganglion cell layer (GCL), oligodendrocyte (ODC) densities ( $P=0.43$ ) and myelin sheath dimensions (g-ratio;  $P=0.99$ ) in the optic nerve were indistinguishable from

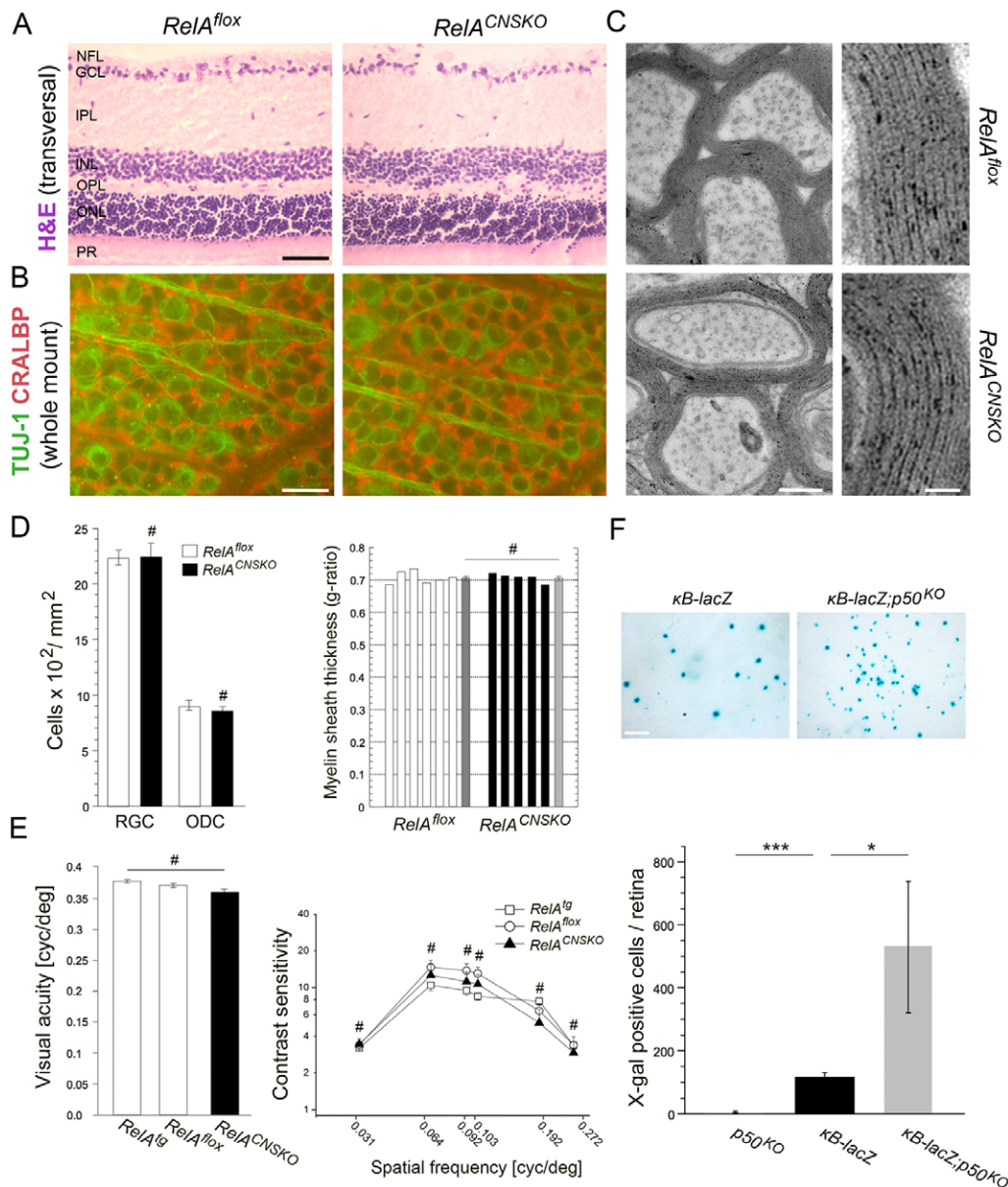


**Fig. 1. Visual system characterization under modulated RelA activity.** (A) HE staining of transversal retina showed normal layer morphology in *RelA<sup>CNSKO</sup>* mice. NFL, nerve fiber layer; GCL, ganglion cell layer; IPL, inner plexiform layer; INL, inner nuclear layer; OPL, outer plexiform layer; ONL, outer nuclear layer; PR, photo receptor layer. Scale bar: 100  $\mu$ m. (B) Co-labeling of retinal whole mounts with the RGC marker TUJ-1 (green) and the Müller glia marker CRALBP (red) exhibited a normal RGC to Müller glia ratio and normal cell contacts in the superficial nerve fiber layer and ganglion cell layer in *RelA<sup>CNSKO</sup>* mice as compared with controls ( $n=3$ ). Scale bar: 50  $\mu$ m. (C) Electron microscopy displayed unimpaired myelin sheaths insulating optic nerve axons in *RelA<sup>CNSKO</sup>* mice as compared with those of controls ( $n=5-6$ ). Scale bars: 150 nm (left), 25 nm (right). (D) Impaired cell differentiation and survival were ruled out by the presence of similar naïve RGC densities ( $P=0.88$ ), ODC numbers ( $P=0.43$ ) and g-ratios ( $P=0.99$ ) in the optic nerve of *RelA<sup>CNSKO</sup>* mice and controls ( $n=5-6$  for each group). (E) Functional parameters revealed physiological values for visual acuity ( $P=0.21$ ) and contrast sensitivity ( $P=0.61$ ) in 3-month-old *RelA<sup>CNSKO</sup>* mice ( $n=5$ ). Data show the mean  $\pm$  s.e.m.; \* $P<0.05$ , \*\*\* $P<0.001$ , # $P>0.05$ . (F) Increased retinal  $\kappa$ B-lacZ reporter activity in  $\kappa$ B-lacZ;*p50<sup>KO</sup>* mice compared with that of controls indicated RelA/NF- $\kappa$ B hyperactivity due to p50 deletion ( $P<0.02$ ;  $n=5$ ). Scale bar: 200  $\mu$ m.

those of controls (Fig. 1D), thus excluding developmental or apoptotic cell loss resulting from RelA deletion in neurons and macroglia. Furthermore, as shown in Fig. 1E, *in vivo* parameters for visual acuity and contrast sensitivity were indistinguishable among *RelA<sup>CNSKO</sup>*, *RelA<sup>fllox</sup>* and *RelA<sup>tg</sup>* (*RelA<sup>fllox</sup>* allele-negative, Cre-recombinase-positive) mice ( $P > 0.05$  for each compared condition), thus confirming that neither the insertion of the transgene alone nor the loss of RelA impaired the functionality of the visual projection.

Similarly, mice with homozygous deletion of p50 (*p50<sup>KO</sup>*) have been described to develop normally (Sha et al., 1995). However, starting at an age of 6 months, they become susceptible to precocious neural degeneration (Lu et al., 2006) and enhanced apoptotic cell death of the visual and acoustic systems (Lang et al., 2006; Takahashi et al., 2007).

### Constitutive NF- $\kappa$ B activity is increased in *p50<sup>KO</sup>* mice

To explore the consequences of transcriptionally inhibitory p50 deletion on canonical NF- $\kappa$ B activity, *p50<sup>KO</sup>* mice were crossed with the  *$\kappa$ B-lacZ* reporter line. In this line, the *lacZ* gene coding for  $\beta$ -galactosidase ( $\beta$ -gal) is driven by multiple NF- $\kappa$ B-binding sites (Schmidt-Ullrich et al., 1996). Compared with  *$\kappa$ B-lacZ* control mice with intact p50 gene expression, double transgenic  *$\kappa$ B-lacZ;p50<sup>KO</sup>* mice revealed a fourfold to fivefold increase in the number of X-gal-positive cells in the retina ( $P < 0.02$ ; Fig. 1F) at just 3 months of age, thus confirming that loss of p50 enhances constitutive NF- $\kappa$ B activity. No signal was detected in age-matched *p50<sup>KO</sup>* mice devoid of the *lacZ* gene (Fig. 1F). Thus, deletion of either NF- $\kappa$ B subunit in *RelA<sup>CNSKO</sup>* and *p50<sup>KO</sup>* mice can dynamically shift transcription towards suppression or activation.

### Optic nerve injury induces NF- $\kappa$ B in different cell types

Optic nerve injury (ONI) induced strong and loco-regional NF- $\kappa$ B activation in cells of superficial retinal layers and in the epicenter of the squeezed optic nerve, as detected in respective whole-mount preparations of  *$\kappa$ B-lacZ* reporter mice (X-gal panels in Fig. 2). The number of X-gal-positive cells in the retina significantly increased by 3-fold and 18-fold by 3 and 10 days after ONI, respectively, as compared with naïve specimens ( $P < 0.01$ ; graph in Fig. 2A). As shown by immunohistochemistry, NF- $\kappa$ B-dependent induction of  $\beta$ -gal occurred in the nuclei of TUJ-1-positive RGCs (Fig. 2B, ONI panels; inset in lower panel). Within the optic nerve, the majority of  $\beta$ -gal-positive nuclei could be ascribed to ODCs expressing the marker protein carbonic anhydrase II (CAII; Fig. 2D, ONI panels; inset in lower right panel). The specificity of the CAII signal was confirmed by lack of immunoreactivity in the non-myelinated head of the naïve optic nerve (Fig. 2D, dotted line in naïve panel). Thus, ONI strongly induced NF- $\kappa$ B activity at the site of axonal damage, as well as in the soma of axotomized RGCs.

Activation of the classical NF- $\kappa$ B pathway for target gene expression involves nuclear translocation of RelA – a process that requires its phosphorylation on serine residues and the exposure of a nuclear localization signal (NLS). Using a Ser536 phospho-specific RelA antibody, we detected substantial RelA phosphorylation in extracts of the optic nerve within 3 h after ONI (Fig. 2C, upper panel;  $n = 3$ ). Notably, pSer536 was not present in the naïve optic nerve, despite its high RelA content (Fig. 2C, upper panel). The specificity of the pSer536 immunosignal was confirmed by the emergence of an equivalent band following TNF treatment of hippocampal neurons (Fig. 2C,

upper panel). Because the post-lesional occurrence of RelA phosphorylation was almost abolished in *RelA<sup>CNSKO</sup>* mice, but was preserved in wild-type mice (Fig. 2C, lower panel), its activation should derive from axons and/or macroglia of the optic nerve lesion site.

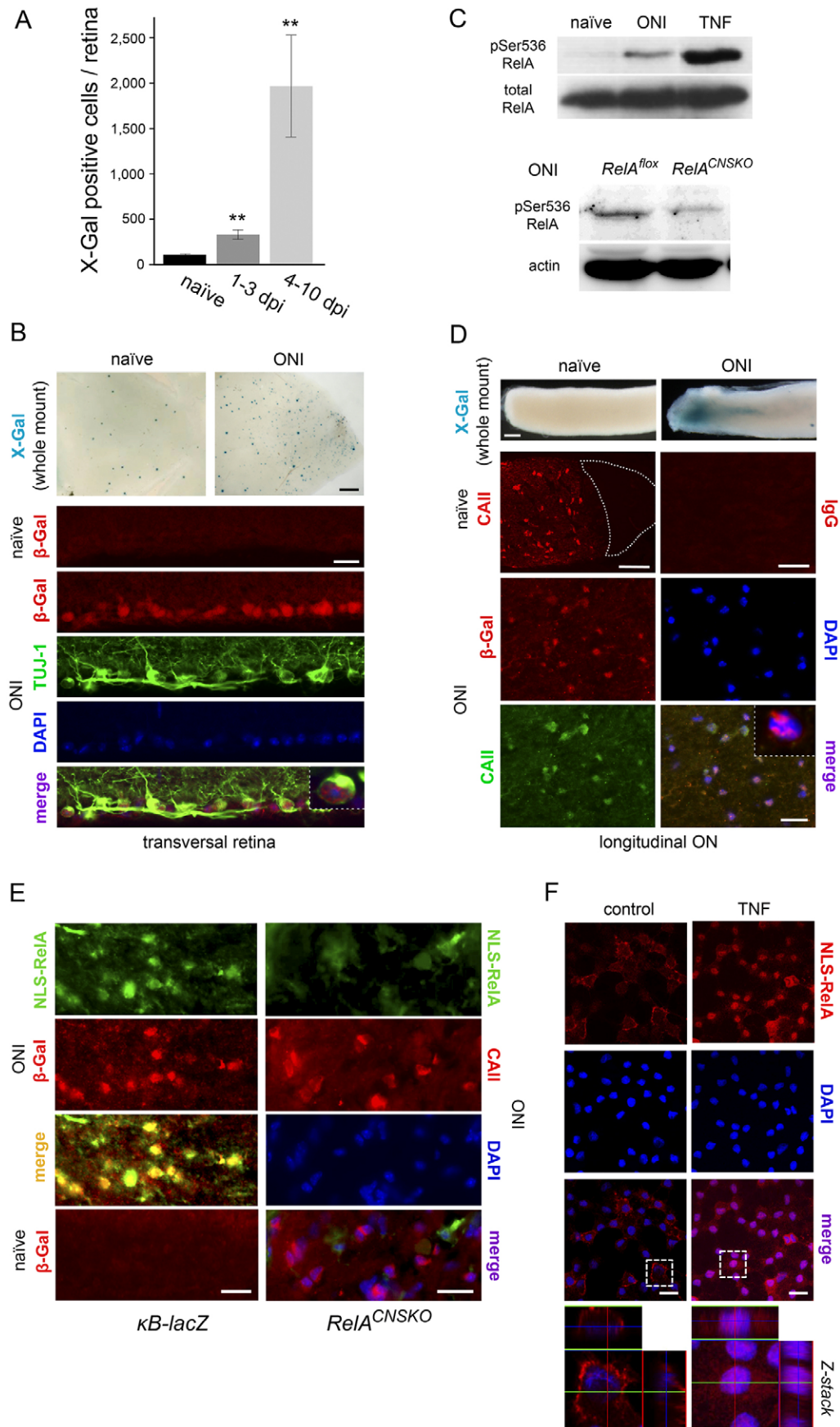
NLS-RelA signal in the injured, but not in the naïve optic nerve, colocalized with the nuclear  $\beta$ -gal immunoreactivity observed in CAII-positive ODCs of  *$\kappa$ B-lacZ* reporter mice, indicating perilesional cytoplasm-to-nucleus translocation of RelA in the majority of  $\beta$ -gal-expressing ODCs (Fig. 2E, left). Such NLS-RelA signal was absent from the nuclei of perilesional CAII-positive ODCs of *RelA<sup>CNSKO</sup>* mice (Fig. 2E, right), confirming the specificity of RelA activation in ODCs. Additionally, we explored the nuclear translocation of RelA in the OLN-93 oligodendrocytic cell line (Richter-Landsberg and Heinrich, 1996) by confocal laser microscopy. As detected by the activation-specific NLS-RelA antibody, nuclei of non-stimulated control cells were free of RelA signal (Fig. 2F, left). Following application of TNF, a prototypical cytokine released during tissue damage, NLS-directed immunoreactivity became strikingly evident in DAPI-positive nuclei of OLN-93 cells (Fig. 2F, right, Z-stack). Similar results were achieved using an antibody directed against the C-terminus of the RelA protein, thus confirming the specificity of the NLS-RelA reactivity (not shown). Collectively, robust steady-state RelA expression in ODCs (not shown), together with induced  $\beta$ -gal reactivity in ODCs (Fig. 2D) indicated that post-lesional RelA activation occurs in ODCs.

### RelA and p50 subunit-dependent RGC survival after injury

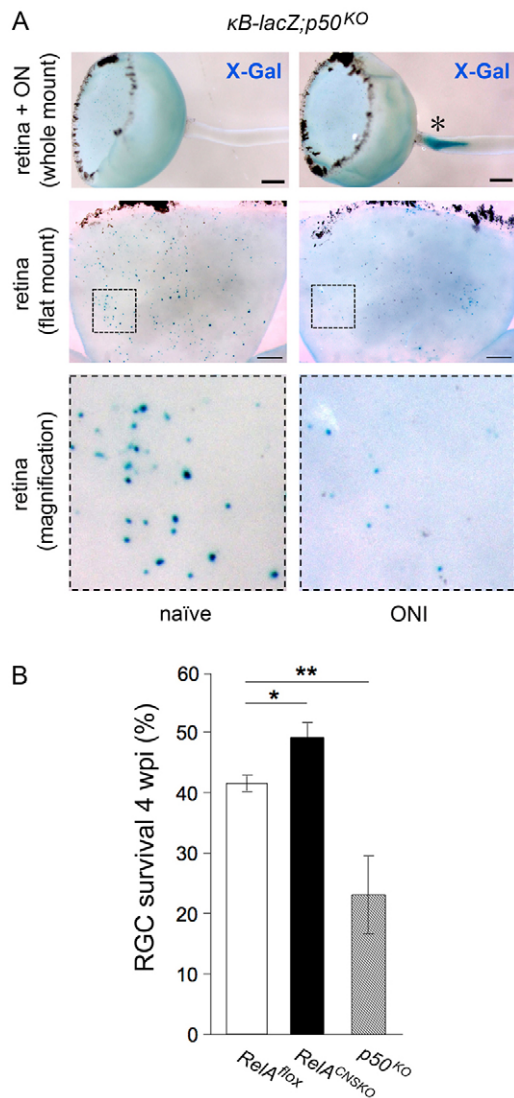
NF- $\kappa$ B activation studies performed on  *$\kappa$ B-lacZ;p50<sup>KO</sup>* reporter mice revealed a strong induction of NF- $\kappa$ B at the site of ONI, as demonstrated by an intense blue color reaction in the X-gal assay. Analysis of the corresponding retina revealed an unexpected reduction in the total number of X-gal-positive cells when analyzed as early as 9 days post-injury (dpi; Fig. 3A;  $n = 3$ ), arguing for enhanced lesion-induced RGC death as a result of p50 deficiency. Because NF- $\kappa$ B has been shown to either inhibit or propagate cell death, we investigated post-lesional RGC survival in *RelA<sup>CNSKO</sup>* and *p50<sup>KO</sup>* mice by assessing TUJ-1 immunoreactivity. Combined neuronal and glial deletion of RelA modestly improved RGC survival after ONI from 42% to 49% ( $P < 0.05$ ) compared with controls. By contrast, the loss of p50 strongly reduced RGC survival, thus resulting in a decrease to 55% of control levels (Fig. 3B;  $P < 0.01$ ). Histologically, retinal atrophy suggested an overall increased susceptibility of CNS neurons to harmful events in *p50<sup>KO</sup>* animals.

### Axonal regeneration is stimulated in *RelA<sup>CNSKO</sup>* mice, whereas p50 deletion triggers Wallerian degeneration

In *RelA<sup>CNSKO</sup>* mice, anterograde cholera toxin B subunit (CTX) tracing (supplementary material Fig. S1) revealed dense bundles of regenerating axons growing into the optic nerve and towards the injury site 4 weeks after ONI (Fig. 4A, upper panel). Robust translesional axon growth beyond the scar and into the distal optic nerve stump was achieved in the majority of optic nerve specimens (81%;  $n = 16$ ). Although not included in software-based quantification owing to their low occurrence (<5% of the total number of regenerated axons, not shown), individual axons spanned a growth distance of 2–3 mm. In control specimens, a substantially lower number of newly generated RGC axons reached the head of the optic nerve, which often lacked intra- or translesional growth aspects (20%;  $n = 10$ ;



**Fig. 2. ONI activates NF-κB in a cell-autonomous manner.** (A) ONI in  $\kappa B$ -lacZ reporter mice increased the number of  $\beta$ -gal-positive cells in the retina by 3-fold at 1–3 days post-injury (dpi) and 18-fold at 4–10 dpi ( $n=3$ ). Data show the mean  $\pm$  s.e.m.;  $**P<0.01$ . (B) Micrographs of retinal whole-mount preparations show increased numbers of X-gal-positive cells (blue) in superficial retinal layers after ONI (upper panel). Transversal retinal sections indicate pan-NF- $\kappa B$  activation in the ganglion cell layer (ONI panel), and colocalization of the  $\beta$ -gal signal (red) with the TUJ-1 staining (green) confirmed NF- $\kappa B$  activation in DAPI-positive (blue) RGC nuclei (purple; inset, 40 $\times$  objective) ( $n=4$ ). Scale bars: 200  $\mu m$  (upper panel), 80  $\mu m$  (lower panels). (C) Immunoblot analysis with total RelA (C-20) and phospho-specific (Ser536) RelA antibodies demonstrated the expression of RelA in naive optic nerve, and activation within 3 h after ONI in wild-type animals (upper panel;  $n=3$ ). TNF-treated hippocampal neurons served as a positive control. Ser536 phosphorylation of RelA was almost completely abolished in RelA<sup>CNSKO</sup> mice (lower panel;  $n=3$ ). (D) Enzymatic X-gal assay of optic nerve (ON) *in toto* preparation revealed NF- $\kappa B$  activation in the lesion epicenter ( $n=6$ ). Colocalization of the  $\beta$ -gal signal (red; ONI panel) with the ODC marker CAII (green) in longitudinal optic nerve sections confirmed NF- $\kappa B$  activation in the DAPI-stained nuclei (blue) of ODCs (purple; inset, 40 $\times$  objective) ( $n=3$ ). Note the absence of CAII reactivity in the non-myelinated optic nerve head (dotted line in naive panel). Scale bars: 100  $\mu m$  (X-gal and naive panels), 30  $\mu m$  (ONI panels). (E) Left: colocalization (yellow) of NLS-RelA-positive cells (green) with  $\beta$ -gal signals (red) in  $\kappa B$ -lacZ reporter mice showed that RelA was the dominant NF- $\kappa B$  subunit activated by ONI in ODCs ( $n=4$ ). Right: no NLS-RelA signal was detectable in the nuclei of CAII-positive ODCs of RelA<sup>CNSKO</sup> mice. Scale bars: 30  $\mu m$ . (F) TNF-induced activation of RelA in oligodendrocytic OLN-93 cells, as detected by NLS-RelA antibody. Z-stack analysis confirmed the nuclear localization of RelA in stimulated cells. Areas enclosed by white dashed lines are shown at higher magnification below. Scale bars: 20  $\mu m$ .



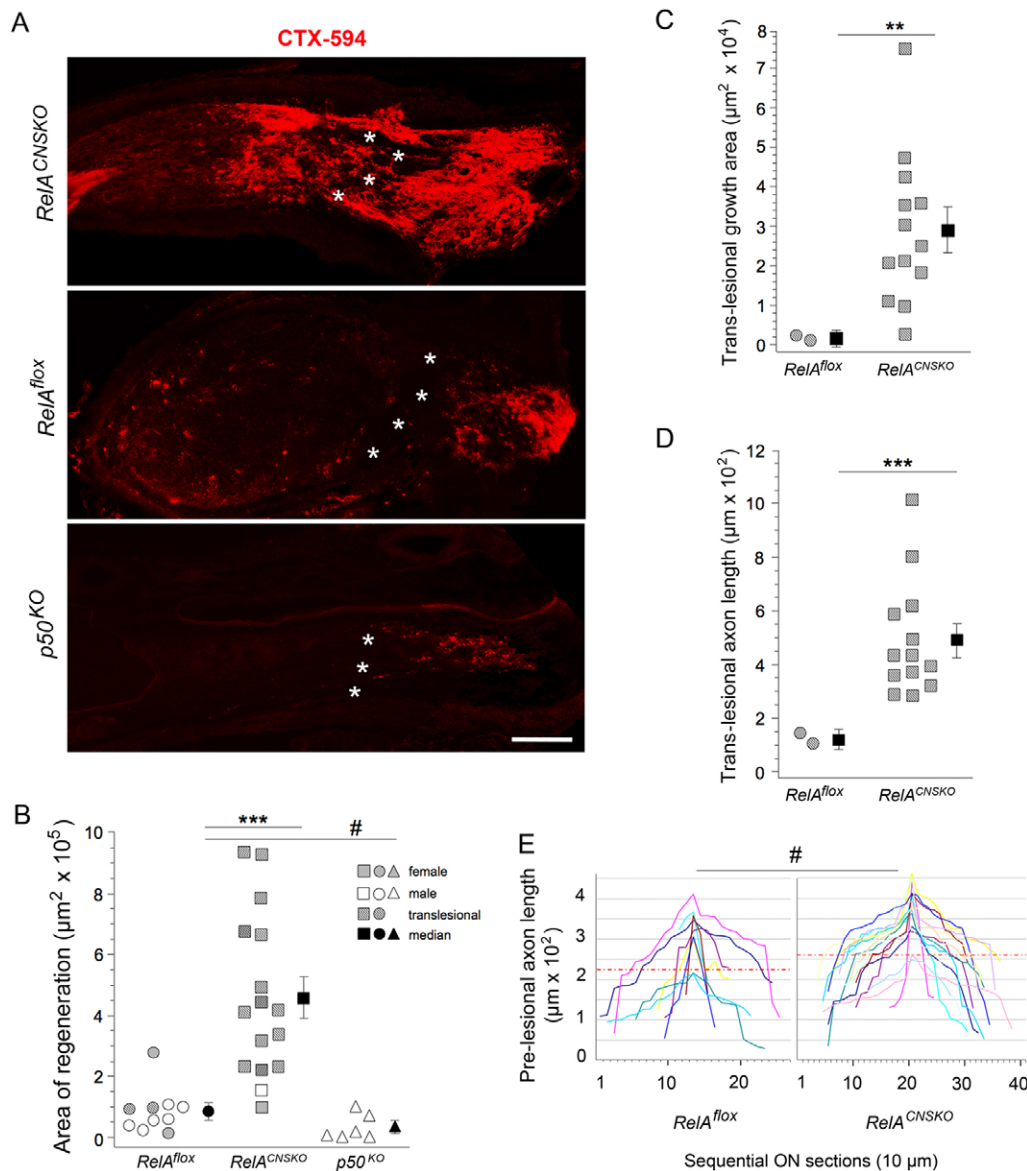
**Fig. 3. RelA and p50 subunits differentially control RGC survival after ONI.** (A) ONI performed on  $\kappa B$ -lacZ; $p50^{KO}$  reporter mice strongly induced NF- $\kappa B$ -dependent X-gal staining (blue) at the optic nerve (ON) injury site (right), which was lacking at the naïve site (left). Asterisk, lesion site. Scale bars: 200  $\mu m$ . Photomicrographs of corresponding flat-mounted retinæ show substantial numbers of X-gal-positive RGCs under naïve conditions and a drastic reduction at 9 dpi. Areas enclosed by black dashed lines are shown at higher magnification below. Scale bars: 200  $\mu m$ . (B) RelA deletion exerts moderate but significant anti-apoptotic effects on RGCs at 4 weeks post-injury (wpi) ( $n=9$  for *RelA<sup>CNSKO</sup>*;  $n=7$  for *RelA<sup>flox</sup>*). By contrast, p50 ablation decreased RGC survival ( $n=3$ ). Data show the mean  $\pm$  s.e.m.; \* $P<0.05$ , \*\* $P<0.01$ .

Fig. 4A, middle). *RelA<sup>tg</sup>* animals similarly showed repressed growth responses (data not shown), thus ruling out a phenotype caused by the presence of the transgene itself. Examination of retinæ from each group excluded the possibility that the apparent lower ingrowth in control samples was a result of lower labeling quality; however, in *RelA<sup>CNSKO</sup>* mice, intraretinal fascicular degeneration appeared to be attenuated. Generally, our histological post-mortem results correlated well with *in vivo* analysis of optic nerve regeneration that was performed using Mn<sup>2+</sup>-enhanced magnetic resonance imaging (MEMRI; supplementary material Fig. S2). The strong crush technique

that was applied in order to avoid fiber sparing resulted in a pronounced axonal dieback as well as a long latency and still rather limited distance of regeneration behind the lamina cribrosa (supplementary material Fig. S2).

Software-based quantitative analysis of longitudinal optic nerve sections detected, on average, a fivefold increase in the extent of axonal regeneration in *RelA<sup>CNSKO</sup>* mice compared with that of controls (*RelA<sup>flox</sup>*,  $85.91 \pm 23.95 \times 10^3 \mu m^2$  versus *RelA<sup>CNSKO</sup>*,  $458.82 \pm 66.65 \times 10^3 \mu m^2$ ;  $P<0.001$ ;  $\pm$  s.e.m.; Fig. 4B). When considering the maximum growth responses in both groups, an even greater stimulation (tenfold) was attained. Further characterization revealed translesional growth areas to be 17-fold increased (*RelA<sup>flox</sup>*,  $1.67 \pm 0.53 \times 10^3 \mu m^2$  versus *RelA<sup>CNSKO</sup>*,  $29.10 \pm 5.57 \times 10^3 \mu m^2$ ;  $P<0.01$ ;  $\pm$  s.e.m.; Fig. 4C) and translesional distances to be fourfold increased (*RelA<sup>flox</sup>*,  $122.55 \pm 0.53 \mu m$  versus *RelA<sup>CNSKO</sup>*,  $487.04 \pm 59.57 \mu m$ ;  $P<0.001$ ; Fig. 4D) in *RelA<sup>CNSKO</sup>* mice compared with those of controls. The fact that the spaces between the optic disc and the lesion site were comparable ( $\sim 240 \mu m$ ) in animals of both groups (*RelA<sup>flox</sup>*, mean 223.68  $\mu m$  versus *RelA<sup>CNSKO</sup>*, mean 263.57  $\mu m$ ;  $P=0.07$ ; Fig. 4E) excluded the possibility that the observed results were artifacts caused by biased position of the injury site. Furthermore, colocalization of GAP-43 with the CTX tracer (Fig. 5A) and the emergence of GAP-43-enhanced rudimentary growth cones (Fig. 5B) emphasized the axoneogenic process in *RelA<sup>CNSKO</sup>* mice. Intraretinally, RGCs elongated MAP2-positive dendritic-like arbors, which grew into deeper retinal layers towards the optic disc (Fig. 5B, right). Such a growth pattern was exclusive to *RelA<sup>CNSKO</sup>* mice, thus suggesting fundamental growth reprogramming with high axonal and dendritic plasticity at the expense of a defined polarized growth shape.

In contrast to the growth improvement in *RelA<sup>CNSKO</sup>* mice, injured optic nerves of *p50<sup>KO</sup>* animals demonstrated negligible regeneration, which was – although not significant – even lower than in controls (Fig. 4A, lower panel; 4B). Of note, *p50<sup>KO</sup>* animals are known to develop normally and possess physiological RGC counts at young mature ages; however, these animals develop age-dependent alterations in axon-myelin structure (Lu et al., 2006; Takahashi et al., 2007). Assuming spontaneous destabilization of axonal integrity in *p50<sup>KO</sup>* mice, we applied the degeneration marker Fluoro Jade and compared the optic nerve cytoskeleton in naïve and lesioned young *RelA<sup>CNSKO</sup>* and *RelA<sup>flox</sup>* mice with that of young and aged naïve *p50<sup>KO</sup>* mice. *RelA<sup>CNSKO</sup>* and control animals remained devoid of any staining under naïve conditions and were indistinguishable with respect to the extent of fiber degeneration at 2 weeks after axonotmesis (Fig. 5C). However, at 10 months, an age at which they are susceptible to neural degeneration, naïve *p50<sup>KO</sup>* mice displayed drastic fiber disintegration and neurofilament breakdown, which was not discernible in age-matched naïve wild-type (not shown) or naïve *RelA<sup>CNSKO</sup>* mice (Fig. 5C, right-most panel). The specificity of the assay was confirmed by negative signals in brain regions adjacent to the intracerebral part of the degenerating optic tract (Fig. 5C, right-most panel). Furthermore, toxic axonopathy elicited 4 weeks after intraocular TNF application (2 ng) resulted in a similar staining pattern to that observed 4 weeks after axonotmesis (not shown). Because RGC quantification in *p50<sup>KO</sup>* mice revealed a drastic decline relative to control cell numbers (Fig. 3B), growth failure in this case is suggested to be also due to reinforced retinal atrophy, including RGC decimation following ONI. These observations highlight the functional polarity of RelA and p50 in axonal degeneration and



**Fig. 4. Axonal regeneration is enhanced in *RelA*<sup>CNSKO</sup> mice.**

(A–D) Axonal regeneration as detected by CTX-594-positive fiber ingrowth into the optic nerve was greatly stimulated in *RelA*<sup>CNSKO</sup> mice ( $n=16$ ) as compared with controls ( $n=10$ ). (A) Translesional fiber elongation was frequently observed in *RelA*<sup>CNSKO</sup> mice, but rarely in controls. Asterisks, lesion site. In *p50*<sup>KO</sup> mice ( $n=6$ ), axon ingrowth into the optic nerve head was even lower than in controls. Scale bar: 100  $\mu\text{m}$ . (B) Quantification of total growth area within individual optic nerves of *RelA*<sup>CNSKO</sup> versus *p50*<sup>KO</sup> and control mice. Gender-related effects were not evident. (C) Selective assessment of translesional growth areas. (D) Absolute translesional axon lengths in *RelA*<sup>CNSKO</sup> mice versus controls. Error bars indicate s.e.m. (E) Measurement of pre-lesional distances indicated comparable positions of the injury site in *RelA*<sup>CNSKO</sup> mice and controls, thus excluding artifacts in real growth distances. ON, optic nerve. Red dashed line indicates the mean distance bridged by regenerating axons between the lamina cribrosa and the injury site. \*\* $P<0.01$ , \*\*\* $P<0.001$ , # $P>0.05$ .

regeneration. Whereas *p50*<sup>KO</sup> mice display a reduced capacity for repair of endogenous or injury-induced fiber damage, fiber integrity and regeneration are stabilized and promoted in *RelA*<sup>CNSKO</sup> mice.

### The pro-regenerative effect of RelA deletion is cell-type dependent

The unexpectedly high expression of RelA in naïve ODCs raised the possibility of a hitherto unrecognized growth-relevant RelA function mediated by an interaction between neurons and growth-inhibitory ODCs. To explore whether the pro-regenerative effect observed in *RelA*<sup>CNSKO</sup> mice was due to the deletion of RelA from RGCs or from ODCs, we deleted RelA specifically in ODCs by using CNP1-promoter-driven Cre recombinase expression (*RelA*<sup>ODCKO</sup>). The activity of CNP1-Cre recombination in the optic nerve was verified in Rosa26R;CNP1-Cre reporter mice by using a colorimetric assay (Fig. 6A). Robust deletion of RelA protein in the optic nerve of *RelA*<sup>ODCKO</sup> mice was further confirmed by immunoblotting (data not shown). In *RelA*<sup>ODCKO</sup> mice, the outgrowth of newly generated axons at 4 weeks after

ONI was significantly enhanced over that of controls by about ninefold (*RelA*<sup>lox</sup>,  $17.59 \pm 9.00 \times 10^3 \mu\text{m}^2$  versus *RelA*<sup>ODCKO</sup>,  $155.53 \pm 46.00 \times 10^3 \mu\text{m}^2$ ;  $P<0.05$ ;  $\pm$ s.e.m.; Fig. 6B), suggesting that RelA ablation in ODCs acts to inhibit the common white-matter-derived growth failure. Because the slow kinetics of Wallerian degeneration in the CNS add to regenerative failure, we investigated the progress of ONI-dependent myelin degradation by assessing the levels of MBP protein. In animals that carry a neuroectodermal RelA deletion (*RelA*<sup>CNSKO</sup>) including RelA loss in ODC, the decline in the levels of structural MBP during Wallerian degeneration was much greater than in controls, which might explain the stimulated axogenesis observed in *RelA*<sup>ODCKO</sup> mice (Fig. 6C;  $n=3$ ). Because the area of regeneration in *RelA*<sup>ODCKO</sup> mice remained lower than that of *RelA*<sup>CNSKO</sup> mice (Fig. 4B), it is possible that additional RelA-deficient cell populations contribute to achieve the maximum growth responses that are observed in animals with combined neuronal and glial RelA deletion.

We further investigated axoneogenesis in mice with conditional astrocyte-specific deletion of RelA (*RelA*<sup>ASTKO</sup>). GLAST-mediated Cre targeting of retina-specific astrocytes (i.e.

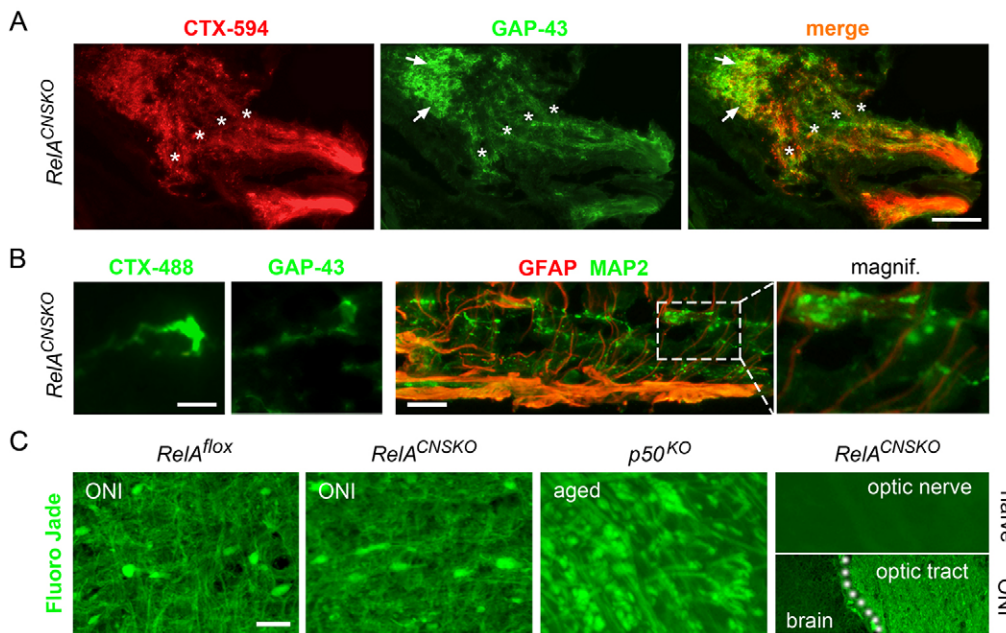


**Fig. 5. Wallerian degeneration is enhanced in  $p50^{KO}$  mice.** (A) CTX-594 (red) colocalized with GAP-43 (green) in elongating axons of  $RelA^{CNSKO}$  mice. Note the strongest GAP-43 signal in axon tips (arrows) beyond the injury site (asterisks). Scale bar: 100  $\mu\text{m}$  (B) Left: in  $RelA^{CNSKO}$  mice, newly elaborated axons developed rudimentary growth cones at their GAP-43-positive tips (green). Scale bar: 15  $\mu\text{m}$ . Right: in retinæ counterstained with GFAP (red) for anatomic orientation, the appearance of aberrant MAP2-positive processes (green) in  $RelA^{CNSKO}$  mice indicated a pro-regenerative influence on RGC dendrites (dashed box with magnification). Scale bar: 30  $\mu\text{m}$ . (C) ONI induced Wallerian degeneration in  $RelA^{CNSKO}$  mice and  $RelA^{fllox}$  controls ( $n=3$ ), as indicated by Fluoro-Jade-reactive axon bulges (green). However,  $p50^{KO}$  mice showed strong spontaneous fiber degeneration at a susceptible age of 10 months, as demonstrated by intense Fluoro Jade staining ( $n=3$ ). Specificity of the signal was indicated by lack of Fluoro Jade reactivity in naïve optic nerve of 10-month-old  $RelA^{CNSKO}$  mice and outside the injured optic tract (right panel). Scale bar: 50  $\mu\text{m}$ .

Müller glia) was verified using animals with a combined tamoxifen (TAM)-inducible GLAST-CreER<sup>T2</sup>/loxP system (Slezak et al., 2007) and Rosa26-YFP reporter expression (YFP;GLAST-CreER<sup>T2</sup>; Srinivas et al., 2001). In their retinæ, all YFP-positive cells, identified as Müller glia by their long processes and strong expression of CRALBP (not shown), showed a profound increase in YFP reporter signal in response to TAM (Fig. 6D, arrows). Following ONI,  $RelA^{ASTKO}$  mice displayed a 19-fold greater area of elaborated axons compared with that of controls ( $RelA^{fllox}$ ,  $17.59 \pm 9.00 \times 10^3 \mu\text{m}^2$  versus  $RelA^{ASTKO}$ ,  $383.31 \pm 57.18 \times 10^3 \mu\text{m}^2$ ;  $P < 0.01$ ; Fig. 6E). This response exceeded the growth stimulation observed in  $RelA^{ODCKO}$  mice but remained below the absolute growth values observed in  $RelA^{CNSKO}$  mice (Fig. 4B). Because chondroitin sulfate proteoglycans (CSPG) secreted by scar-forming astrocytes are chemically repulsive and mechanically impenetrable growth inhibitors, we investigated post-lesional neurocan secretion in  $RelA^{CNSKO}$  mice. Neurocan produced within the lesion epicenter in  $RelA^{CNSKO}$  mice was less dense and less compacted than in controls at 10 days (Fig. 6F) and 4 weeks (not shown) after ONI. Consequently, axons elaborated from  $RelA^{CNSKO}$  mice grew directly into and beyond the scar, whereas, in controls, the growth of most of the axons was arrested when they reached the scar region (Fig. 6G, arrows), thus suggesting the RelA-dependent expression of repulsive scar constituents. Importantly, invasion of F4/80<sup>+</sup> CD11b<sup>+</sup> microglia and macrophages into the injury region was indiscernible between the two groups (not shown). Therefore, a difference mediated by immune-privileged CNS functions seems unlikely. In summary, the enhanced post-lesional axonal regeneration observed in  $RelA^{CNSKO}$  mice compared with that of controls cannot be explained by RelA deletion in

oligodendrocytes ( $RelA^{ODCKO}$ ) or astroglia ( $RelA^{ASTKO}$ ) alone, but might involve further cell-type-specific (in particular, neuron-intrinsic) molecular mechanisms.

#### RelA-associated regeneration parallels cell-type-specific Cdh1 suppression

Given the results reported above, we next examined whether the axonal growth regulator Cdh1, which was found expressed in the naïve mature cortex and retina (Fig. 7A), where it localizes to RGCs (Fig. 7B), is upregulated during RelA-mediated growth suppression. This hypothesis was reinforced by the fact that the highest levels were found in myelin-enriched projecting fibers of the optic and sciatic nerves (Fig. 7A). Following ONI, Cdh1 levels declined by 50% in the retinæ of regeneration-competent  $RelA^{CNSKO}$  mice but rose to 182% in non-regenerating  $RelA^{fllox}$  mice compared with the levels in uninjured controls (Fig. 7C). By contrast, Cdh1 was upregulated to 220% and 225% in young adult  $p50^{KO}$  mice after ONI and in the spontaneously degenerating retina of aged 10-month-old  $p50^{KO}$  mice, respectively (Fig. 7C). Assuming that neuronal Cdh1 content defines the threshold for regeneration and degeneration, and that Cdh1 levels are modulated by pro- or anti-regenerative inputs from ODCs and astrocytes, Cdh1 levels should be equally, but weaker, suppressed in  $RelA^{ODCKO}$  and  $RelA^{ASTKO}$  mice compared with  $RelA^{CNSKO}$  mice. Accordingly, Cdh1 levels were found to be reduced in all growth-stimulating knockout lines, with the strongest suppression (by 47%) in the most highly regenerating  $RelA^{CNSKO}$  and  $RelA^{ASTKO}$  mice, as compared with a 20% reduction in expression in  $RelA^{ODCKO}$  mice (Fig. 7D). In addition, the physiological inhibitor of Cdh1, EMI1 (early mitotic inhibitor 1), was upregulated (by 40%) in naïve retinæ of  $RelA^{CNSKO}$  mice,

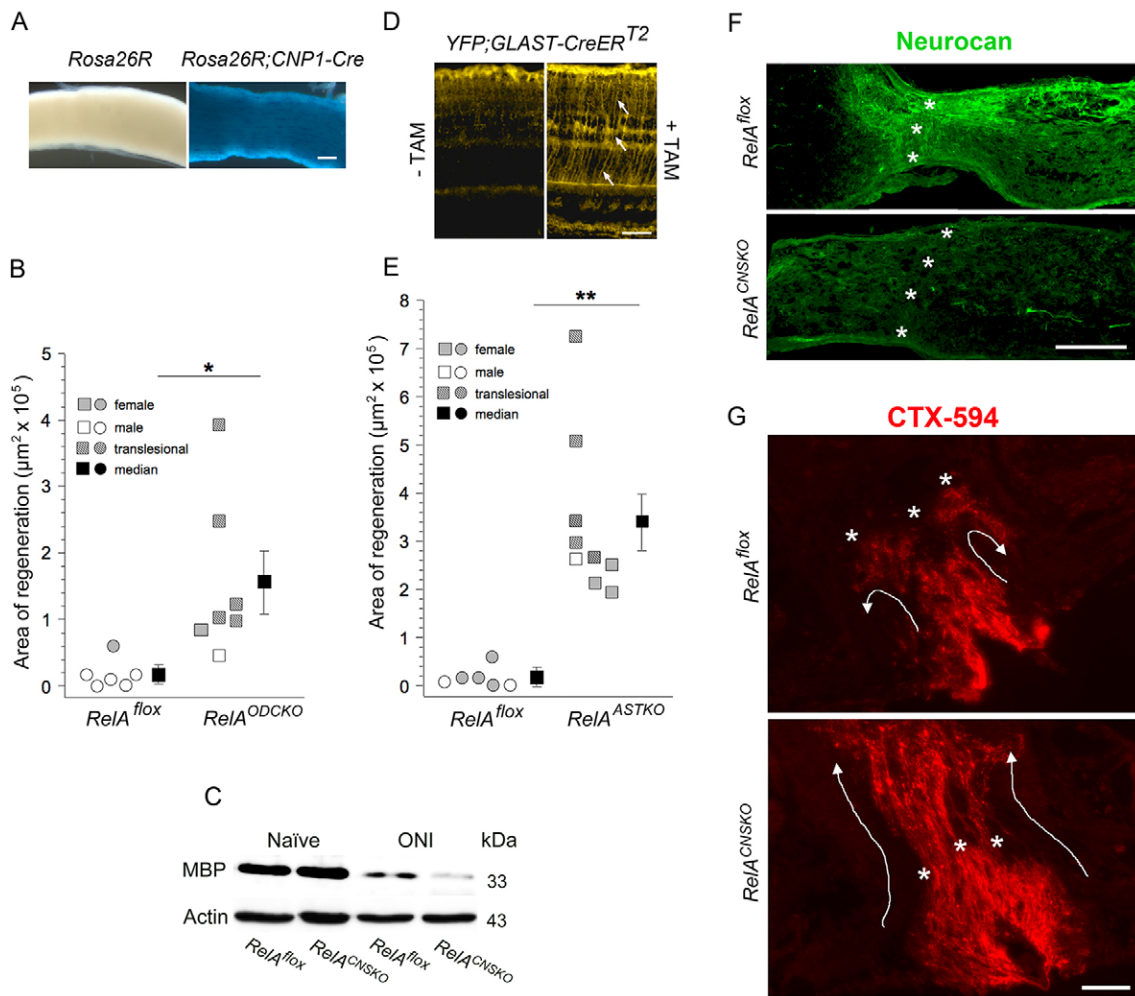


**Fig. 6. RelA differentially modulates axonal regeneration in *RelA<sup>CNSKO</sup>*, *RelA<sup>ODCKO</sup>* and *RelA<sup>ASTKO</sup>* mice.** (A) CNP1-Cre activity in the optic nerve of *RelA<sup>ODCKO</sup>* mice was confirmed by its intense blue staining in *Rosa26R;CNP1-Cre* reporter mice. Scale bar: 100  $\mu\text{m}$ . (B) RelA deletion selectively in ODCs (*RelA<sup>ODCKO</sup>*) significantly enhanced axonal regeneration. Error bars show s.e.m. (C) Accelerated degradation of white matter MBP was observed in *RelA<sup>ODCKO</sup>* mice at 4 weeks after ONI (two independent runs using pooled protein of three animals). (D) Deletion of RelA in Müller glia (arrows) was confirmed by YFP induction in *YFP;GLAST-CreER<sup>T2</sup>* reporter mice after tamoxifen (TAM) treatment. Scale bar: 50  $\mu\text{m}$ . (E) The pro-regenerative effects of RelA deletion in astrocytes (*RelA<sup>ASTKO</sup>*) exceeded those observed in *RelA<sup>ODCKO</sup>* mice. Error bars show s.e.m. (F) Growth-promoting effects paralleled a reduced production of repulsive neurocan at the injury site ( $n=3$ ). Scale bar: 250  $\mu\text{m}$ . (G) In *RelA<sup>CNSKO</sup>* mice, regrowing axons penetrated the scar region more easily, as shown by CTX labeling ( $n=16$  for *RelA<sup>CNSKO</sup>*;  $n=10$  for controls). Asterisks, scar region. Arrows delineate preferred growth direction of newly built axons. Scale bar: 150  $\mu\text{m}$ .

whereas it was downregulated (30%) in aged and non-regenerating *p50<sup>KO</sup>* mice (Fig. 7E). ONI further induced a twofold to threefold upregulation of EMI1; however, this induction was independent of the genotype (273% of naïve levels in *RelA<sup>fllox</sup>* versus 221% of naïve levels in *RelA<sup>CNSKO</sup>*). These data show that Cdh1 levels are negatively correlated with the occurrence of successful regrowth in mature neurons and they support the notion that the APC<sup>Cdh1</sup> cascade is involved in the NF- $\kappa$ B-dependent ambivalent regulation of axonal restoration and degradation.

#### RelA deletion causes an inactivating shift in the subcellular localization of Cdh1

We next examined RelA-associated post-translational modifications of Cdh1. Because the phosphorylation and subsequent shift of stabilized Cdh1 from the nucleus to the cytoplasm indicates its inactivation (Huynh et al., 2009), we

investigated its subcellular distribution in wild-type and RelA-deficient hippocampal neurons during axogenesis (Fig. 7F–H). Similar to naïve RGCs *in vivo* (Fig. 7B), the hippocampal neurons of controls showed a common mixed nuclear and cytoplasmic localization of Cdh1 (Huynh et al., 2009), although with a nuclear dominance (Fig. 7F–H). In the absence of RelA, a twofold relative increase in the amount of cytoplasmic Cdh1 occurred (*RelA<sup>fllox</sup>*,  $19.4 \pm 1.8\%$  versus *RelA<sup>CNSKO</sup>*,  $40.8 \pm 3.7\%$ ;  $P < 0.001$ ;  $\pm$ s.e.m.; Fig. 7F–H). Neurons with a cytoplasmic Cdh1 preponderance above 70% were almost exclusively restricted to *RelA<sup>CNSKO</sup>* mice (Fig. 7H). Strong staining against the axo-neuronal marker TUJ-1 indicated neuronal viability and axonal vitality under both conditions (Fig. 7F), irrespective of their RelA-dependent Cdh1 content.

As a further target for RelA-mediated Cdh1 regulation, we investigated the protein levels of the HLH-related pro-regenerative Id2. Because Id2 is a nuclear target, we looked for a pro-nuclear

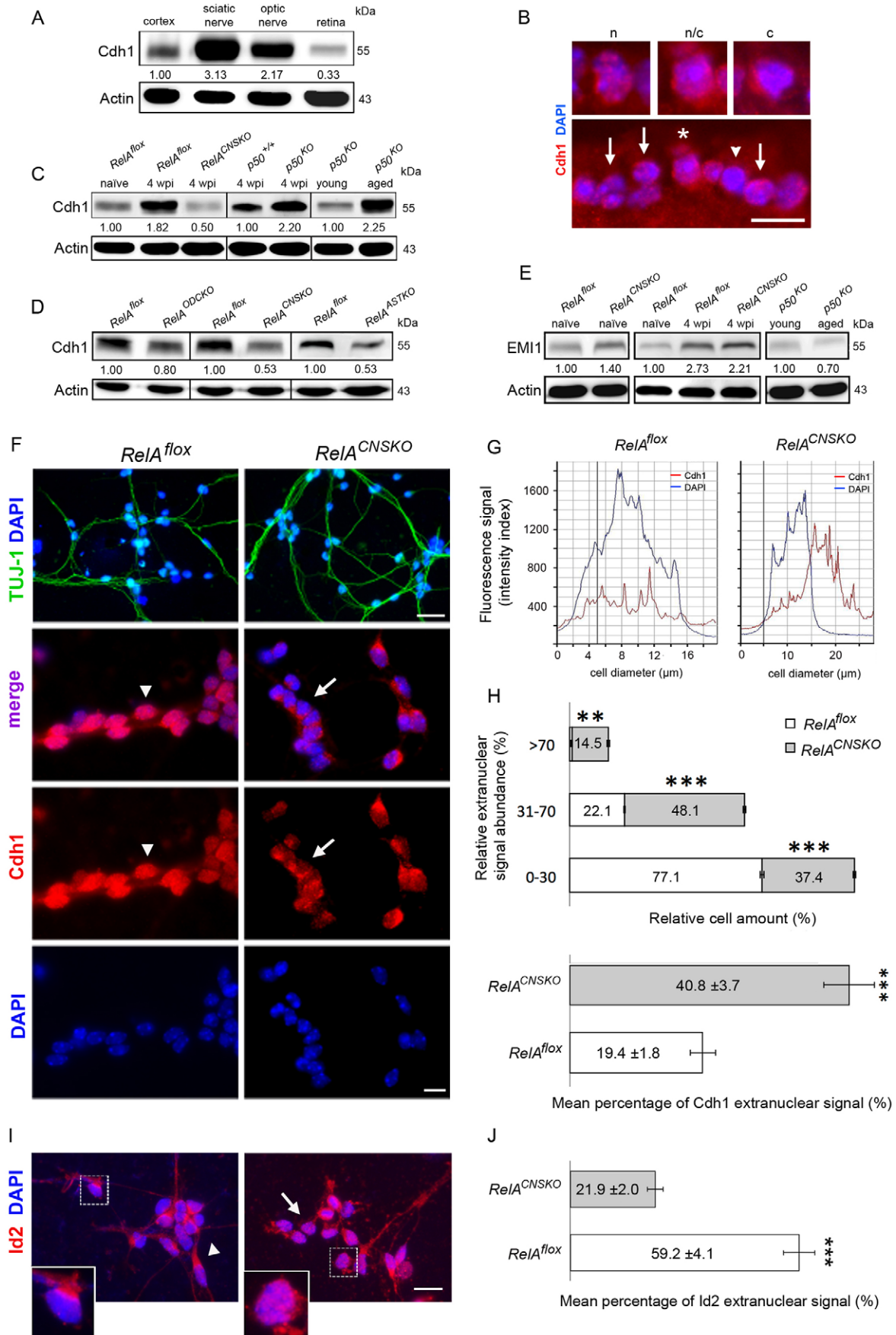


Fig. 7. See next page for legend.

**Fig. 7. RelA controls Cdh1 levels and its nucleo-cytoplasmic shuttling.** (A–D) Cdh1 acts in neurons to control RelA-dependent axon growth. (A) The expression of Cdh1 was increased in naïve optic and sciatic nerves and, to a lesser extent, in cortex and retina ( $n=3$ ; pooled protein from three animals). Calculations indicate densitometry readings relative to that of the actin loading control. (B) Within the naïve retina, Cdh1 was localized to RGCs and displayed a nuclear (n; arrows), cytoplasmic (c; arrow head) or mixed (n/c; asterisk) distribution. Scale bar, 50  $\mu\text{m}$ . (C) Cdh1 upregulation in wild-type retinae at 4 weeks post-injury (wpi) was suppressed in  $RelA^{CNSKO}$  mice ( $n=4$ ; three samples). By contrast, Cdh1 was upregulated in growth-incompetent  $p50^{KO}$  mice at 4 weeks post-injury, as well as in progeroid retinae at the age of 10 months ( $n=3$ ; two samples). (D) In growth-conditioned retinae, Cdh1 was found to be suppressed as a function of the cell type targeted by RelA deletion. The degree of Cdh1 decline (in terms of Cdh1 levels,  $RelA^{CNSKO} \approx RelA^{ASTKO} < RelA^{ODCKO}$ ) correlated with absolute growth responses ( $n=4$ ; three samples). (E) The Cdh1 inhibitor EM1 was upregulated in naïve  $RelA^{CNSKO}$  mice. ONI caused no further induction ( $n=3$ ; three samples). Corresponding to increased Cdh1 levels, EM1 levels declined with aging in  $p50^{KO}$  mice ( $n=3$ ; two samples). (F–H) RelA defines nucleo-cytoplasmic shuttling of Cdh1 in cultured hippocampal neurons. (F) Co-staining for Cdh1 and nuclear DAPI in hippocampal neurons (4 days *in vitro*) revealed a predominantly nuclear (active) localization of Cdh1 in wild-type cells (left, purple nuclei; arrowhead), whereas RelA deletion caused a shift of Cdh1 to a cytoplasmic (inactive) localization (right, blue nuclei; arrow). Solid neuro-neuritic TUJ-1 staining indicated viability of either culture (upper panel;  $n=3$ ). Scale bars: 30  $\mu\text{m}$  (upper panel), 10  $\mu\text{m}$  (lower panels). (G) Nucleo-cytoplasmic shift of Cdh1 in RelA-deficient hippocampal neurons was assessed by cellular immunofluorescence absorption profiles. Both graphs indicate the preponderance of extranuclear inactive Cdh1 in  $RelA^{CNSKO}$  as compared with  $RelA^{fllox}$ . (H) Quantitative analysis of the average cytoplasmic Cdh1 signal distribution (cell numbers:  $RelA^{fllox}$ ,  $n=122$ ;  $RelA^{CNSKO}$ ,  $n=131$ ). Analysis of the cytoplasmic-to-nuclear signal ratio showed that a high percentage of controls (77.1%) had low cytoplasmic Cdh1 signal (0–30%), whereas the majority of  $RelA^{CNSKO}$  cells (48.1%) had a higher cytoplasmic Cdh1 signal (31–70%). Data show the mean  $\pm$  s.e.m. (I) Representative images of cytoplasmic Id2 signal distribution in  $RelA^{fllox}$  and  $RelA^{CNSKO}$  hippocampal neurons (3.5 days *in vitro*), revealing a predominantly cytoplasmic accumulation of Id2 in the axon hill (left; arrowhead and inset) of wild-type cells, whereas RelA deletion caused its nuclear (active) localization (right; arrow and inset). Scale bar: 10  $\mu\text{m}$ . (J) Quantification of subcellular signal distribution showed predominantly cytoplasmic Id2 in controls (59.2%), whereas  $RelA^{CNSKO}$  populations contained predominantly nuclear Id2 (78.1%). Cell numbers:  $RelA^{fllox}$ ,  $n=90$ ;  $RelA^{CNSKO}$ ,  $n=130$ ). Data show the mean  $\pm$  s.e.m.; \*\* $P<0.01$ , \*\*\* $P<0.001$ .

shift in active Id2 in the hippocampal neurons of  $RelA^{CNSKO}$  mice with reduced Cdh1 content. Immunocytochemical and subcellular analysis revealed a predominantly cytoplasmic localization of Id2 in wild-type hippocampal neurons with characteristic accumulation in the axon hill (Fig. 7I, arrowhead and inset), displaying a mean extranuclear signal of  $59.2 \pm 4.1\%$  (Fig. 7J). By contrast, in  $RelA^{CNSKO}$  neurons, Id2 immunoreactivity was concentrated in the DAPI-positive nuclei (Fig. 7I), and the mean percentage of extranuclear signal was reduced to  $21.9 \pm 2.0\%$  (Fig. 7J). Thus, the average nuclear Id2 content was augmented by  $\sim 100\%$  ( $RelA^{fllox}$ , 40.8% versus  $RelA^{CNSKO}$ , 78.1%;  $P<0.001$ ), suggesting that reduced Cdh1 activity stabilized nuclear Id2 steady-state levels. Because total protein content might not reflect this regulation (Kim et al., 2006), immunocytochemistry was preferred over immunoblot analysis of whole-cell lysates. Further studies will aim to identify the growth-responsive target genes that are regulated by this RelA/p50–EM1–APC<sup>Cdh1</sup>–Id2 pathway.

## DISCUSSION

There is accumulating evidence that RelA is crucial for axon formation during embryonic neural development (Gavaldà et al.,

2009). In cervical superficial ganglia, enhanced site-specific Ser536 phosphorylation of RelA in the presence of p50 impairs increases in neurite length and complexity (Gutierrez et al., 2008), whereas RelA suppression by overexpression of either p50 or a dominant-negative I $\kappa$ B $\alpha$  super-repressor in newborn hippocampal neurons results in complete growth arrest (Imielski et al., 2012). It has been suggested that modification of both I $\kappa$ B $\alpha$  and activated RelA determines a functional switch from growth inhibition to growth promotion (Gavaldà et al., 2009; Gutierrez et al., 2008). Moreover, as recently exemplified for hippocampal neurogenesis, the balance between transactivation-competent and -incompetent NF- $\kappa$ B subunits might also be crucial for axogenesis (Imielski et al., 2012). However, such previous experiments were based on *in vitro* analysis of premature PNS and newborn hippocampal neurons. At present, the relevance of NF- $\kappa$ B for structural restoration in the mature post-lesional CNS is undefined, and both subunit-specific and cell-type-specific features of NF- $\kappa$ B activation remain unclear. In this study, we investigated the importance of NF- $\kappa$ B for axonal regeneration and degeneration (i) in mature neurons, (ii) in the CNS, (iii) *in vivo*, (iv) after axonal injury, (v) in a cell-autonomous manner and (vi) in the context of the interdependence between the NF- $\kappa$ B subunits that are dominant in the CNS, RelA and p50.

Apart from the induction of p50 and RelA that has already been demonstrated for severed RGCs (Choi et al., 1998; Takahashi et al., 2007), ONI elicited a previously unrecognized activation of RelA in macroglia. To the best of our knowledge, this is the first time that ODCs, as prototypical CNS growth inhibitors, have been shown to induce the activation of RelA in response to injury. Thus, RelA activation in ODCs might play a crucial role in the cell-autonomous regulation of axonal demyelination and remyelination following axonal injury. This might depend on the type of injury, because in a cuprizone model, the ablation of IKK $\beta$  in astrocytes – but not in ODCs – was sufficient to prevent toxic demyelination (Raasch et al., 2011). Furthermore, in agreement with Brambilla and colleagues (Brambilla et al., 2005), we have confirmed that reactive astroglia of the scar region are a growth-relevant source of NF- $\kappa$ B activation. In their study, NF- $\kappa$ B was inhibited in astrocytes by GFAP-dependent overexpression of an I $\kappa$ B $\alpha$  super-repressor. Whereas this approach does not discriminate between subunit-specific roles, we now have specified RelA as one of the subunits involved in astroglial scar formation and growth suppression. Thus, in addition to the well-characterized role of NF- $\kappa$ B in immune cells for neuron-axonal integrity (Emmanouil et al., 2009), our data emphasize the significance of RelA for axonal renewal by its regulation in CNS-intrinsic neuroectodermal neurons and macroglia. Inhibition of such RelA activation either in astrocytes or ODCs, or in neurons and macroglia together, elicited a graded cell-type-specific stimulation of axon regrowth. The robust growth stimulation in any of these models of RelA depletion – displaying a 5-fold to 19-fold relative increase over controls and an absolute increase in growth in  $RelA^{CNSKO}$  that exceeded that observed in  $RelA^{ASTKO}$ , which, in turn, was greater than that of  $RelA^{ODCKO}$  – points to multimodal positive effects exerted synergistically by the suppression of tonic growth inhibitors from myelin, glial scar tissue and severed RGCs and axons. The growth stimulation in  $RelA^{ODCKO}$  mice coincided with pronounced degradation of MBP protein in the lesioned optic nerve, a finding that is suggestive of accelerated Wallerian degeneration in  $RelA^{ODCKO}$  mice and, thus, reconstitution of a

more permissive post-injury milieu. This is in accordance with the previously described RelA-dependent activation of the MBP promoter in response to TNF stimulation (Huang et al., 2002) and might have implications for demyelination and remyelination in various myelin-related disorders.

The growth-promoting influence of ODC-specific RelA deletion was less than that induced by the loss of RelA from astrocytes. Mechanistically, the enhanced regeneration in *RelA<sup>ASTKO</sup>* mice correlated with a diminished production of CSPG at the lesion site, suggesting that the loss of RelA from astrocytes facilitates growth events that penetrate through the glial scar and restores a target-directed growth orientation. Brambilla and colleagues have identified that the expression of a dominant-negative form of  $\text{I}\kappa\text{B}\alpha$  in scar-forming astrocytes improves functional recovery following SCI (Brambilla et al., 2005; 2009). Here, our GLAST-Cre model suggests that further benefit can be achieved by inhibiting RelA not only in astrocytes of the optic nerve, but also in Müller glia of associated retinae. Owing to the most comprehensive RelA deletion in the nestin-Cre mouse line, which implies loss of RelA in all macroglia populations, RGC numbers in *RelA<sup>ODCKO</sup>* and *RelA<sup>ASTKO</sup>* mice were not expected to deviate from basal RGC counts calculated for *RelA<sup>CNSKO</sup>* mice and, thus, are unlikely to be the reason for the moderate differences in regeneration. That the most effective regeneration was observed in *RelA<sup>CNSKO</sup>* mice implicates neuron-intrinsic RelA effects when reciprocal communication between neurons and glia is present. Ongoing studies on RGC- and neuron-specific knockout mice will further elucidate temporal and spatial interactions between neurons and glia.

The increase in axonal outgrowth in *RelA<sup>CNSKO</sup>* mice that was evident from histological studies was confirmed by additional tract-specific contrast-enhanced MRI techniques performed *in vivo* (supplementary material Fig. S2; Haenold et al., 2012; Fischer et al., 2014). Ongoing long-term studies using repetitive MRI of the visual projection might delineate whether these axons become connected with midbrain targets (as recently claimed by Benowitz's group) in a manner dependent upon cAMP- and PTEN-regulated oncomodulin (De Lima et al., 2012).

Growth modulation by NF- $\kappa$ B was highly subunit specific, because abrogation of the RelA-binding partner p50 did not show any pro-regenerative effect, but rather destabilized axonal integrity. Moreover, naïve *p50<sup>KO</sup>* animals exhibited signs of precocious retinal atrophy as early as 10 months after birth, followed by severe cytoskeletal disintegration and functional visual impairments (data not shown). Such detrimental consequences are in line with the spontaneous degenerative process recently described for aging p50-deficient animals (Lang et al., 2006; Takahashi et al., 2007). Collectively, the balance between p50 and RelA appears to be important to stabilize axons on the structural and functional level. In the absence of RelA, p50 cannot compensate for the lack of transcriptional regulation by RelA. In addition to the loss of function that results from the absence of the interaction between p50 and RelA, growth might be stimulated by the interaction of p50 with novel dimerization partners, such as Bcl-3 or c-Rel. We are currently generating neuro-ectodermal *RelA*;*c-Rel* double-knockout mice to establish whether the pro-regenerative response is further enhanced or diminished. By contrast, in *p50<sup>KO</sup>* mice, the lack of its suppressor function might result in the establishment of pro-apoptotic or pro-degenerative gene expression profiles. Whether reactive NF- $\kappa$ B induction in *p50<sup>KO</sup>* mice – as shown for retinae – also occurs in ODCs and astrocytes of the optic nerve and thus contributes to

the modulation of growth responses will be addressed in future studies.

The transcriptional changes controlled by RelA and p50, which influence axogenesis and axonal degeneration, are still undefined. Interestingly, inhibition of Cdh1, a co-activator for the E3 ubiquitin ligase anaphase-promoting complex/cyclosome (APC/C), in embryonic primary cultures can enhance axon elaboration and override the growth suppression mediated by myelin factors (Konishi et al., 2004). In cycling cells, Cdh1 promotes ubiquitylation and degradation of cell-cycle regulators such as cyclins and Cdh1 itself. Transcriptional repression of Cdh1 by upregulation of the Smad-interacting protein-1 (SIP1, also known as ZEB2) influences growth arrest and senescence, e.g. upon TNF-mediated NF- $\kappa$ B activation (Chua et al., 2007; Katoh and Katoh, 2009). Notably, APC<sup>Cdh1</sup> expression has been shown to remain particularly high in the nuclei of post-mitotic neurons. Here, analysis of Cdh1 in naïve CNS tissue indicated that it is expressed in the retina and cortex, as well as in myelin-enriched axonal projections, thus complementing the previously described expression of Cdh1 in astrocytes (Herrero-Mendez et al., 2009). In accordance with its anti-growth function, retinal levels of Cdh1 were suppressed in growth-permissive *RelA<sup>CNSKO</sup>* mice following ONI. In the different cell-type-specific RelA knockout lines, the best pro-regenerative effect paralleled the greatest Cdh1 decline, whereas Cdh1 levels increased in growth-incompetent retinae of *p50<sup>KO</sup>* mice. Therefore, our data suggest that Cdh1 is a CNS-specific downstream target of RelA and possibly of p50, which can regulate growth responses by balancing intranuclear Cdh1 levels. In support of this molecular interaction, the F-box only protein EMI1, which physiologically functions as a negative regulator of Cdh1, showed the reverse pattern of expression, being upregulated in growth-conditioned *RelA<sup>CNSKO</sup>* mice, but downregulated in growth-incompetent *p50<sup>KO</sup>* mice.

These observations make Cdh1 and its coupling to NF- $\kappa$ B activity a strong candidate for integrating extra- and intra-neuronal growth signals in the mature CNS, followed by either a positive or negative growth response. The reduced and predominantly cytoplasmic (i.e. inactive) Cdh1 protein content observed in *RelA<sup>CNSKO</sup>* mice supports the possibility of a RelA-dependent mechanism of Cdh1 inactivation with consequent growth stimulatory function. By contrast, stabilized Cdh1 levels in the retinae of *RelA<sup>fllox</sup>* mice coincided with enhanced nuclear Cdh1 accumulation. As a further line of evidence for this pathway, the Cdh1 substrate Id2 was stabilized in the nuclei of *RelA<sup>CNSKO</sup>* neuronal cultures. Increases in the steady-state levels of Id2, either as a result of the overexpression of a ubiquitylation-resistant D-box mutant or of Cdh1 knockdown, have been reported to stimulate the axonal outgrowth of immature neurons and to enhance the regeneration of dorsal root ganglion neurons after SCI (Lasorella et al., 2006; Yu et al., 2011). As for Cdh1, its pro-regenerative effects might only partly depend on the processes of ubiquitylation and proteasomal degradation that are essential for cell-cycle control (e.g. by cyclins) – CNS-specific regulatory mechanisms might also be involved. Studies on fractionated cell extracts will further elucidate the role of Id2 in growth control.

In summary, our results support a novel mechanism that controls axonal self-renewal and Wallerian degeneration in the adult CNS in a dual manner, by the highly subunit- and cell-type-specific regulation of a RelA/p50–EMI1–APC<sup>Cdh1</sup>–Id2 cascade. Whereas recent data on the influence of NF- $\kappa$ B or Cdh1 on axonal growth were acquired from cultured and immature

neurons, our study addresses open questions on their capacity to regulate growth *in vivo* and in the mature CNS, and extends the current knowledge on NF- $\kappa$ B and Cdh1 to the pathophysiology of neurodegenerative and traumatic CNS diseases.

## MATERIALS AND METHODS

### Transgenic mice

For regeneration studies, 14–18-week-old mice with a homozygous Cre/loxP-based deletion of *relA* alleles (*RelA<sup>fl/fl</sup>;tg/+*) and floxed littermate controls (*RelA<sup>fl/fl</sup>;+/+*, designated *RelA<sup>lox</sup>*) were used. Conditional *RelA<sup>lox</sup>* mice were a kind gift from Roland M. Schmid (Technical University Munich, Germany) (Algül et al., 2007). The nestin-Cre mouse line was obtained from The Jackson Laboratory (Bar Harbor, ME). Animals were backcrossed to a C57Bl/6 (B6) background for at least ten generations. Oligodendrocyte-specific *RelA* deletion was achieved by CNP1 promoter-driven Cre activity in *RelA<sup>ODCKO</sup>* mice (Lappe-Siefke et al., 2003) and was verified in Rosa26R;CNP1-Cre double transgenic reporter animals carrying a lox-STOP-lox cassette (Soriano, 1999). In these animals, the loci of Cre expression can be monitored by *lacZ*-sensitive colorimetric assay. For astrocyte-specific *RelA* ablation (*RelA<sup>ASTKO</sup>*), a GLAST-driven and tamoxifen-inducible CreER<sup>T2</sup>/loxP system was employed (Slezak et al., 2007). Deletion was induced as published previously (Slezak et al., 2007). Constitutive knockout animals, lacking the p50 subunit (*p50<sup>KO</sup>*) by insertion of a pGK-neo cassette into exon 6 on a B6 background (Sha et al., 1995), and B6 wild-type controls were used at an age of either three or 10 months. Pan-NF- $\kappa$ B activation was assessed using the  *$\kappa$ B-lacZ* reporter line (Schmidt-Ullrich et al., 1996).

Animals were kept under controlled conditions in a pathogen-free environment and provided with food and water *ad libitum*. All animal interventions were performed under deep anesthesia and in accordance with the European Convention for Animal Care and Use of Laboratory Animals and were approved by the local ethics committee.

### Acute CNS injury and tracer applications

The optic nerve was squeezed immediately behind the posterior eye pole with small tilted forceps for 10 s. Eyes which developed ocular pathology or ischemia (e.g. corneal opaqueness, retinal atrophy, congestive bleeding, cataract or lipofuscin deposits) were excluded. In this model of axonotmesis, preserved myelin sheaths serve as guidance structures for outgrowing axons (Misantone et al., 1984).

Optic nerve fiber regeneration was evaluated by a dual anterograde tracing protocol: 2–3 days prior to ONI, 2  $\mu$ l of FITC-conjugated CTX (CTX-488; 1  $\mu$ g/ $\mu$ l; C-22842, Molecular Probes/MoBiTec, Goettingen, Germany) were intravitreally injected, followed by intravitreal application of complementary Cy3-labeled CTX (2  $\mu$ l of CTX-594; 1  $\mu$ g/ $\mu$ l; C-22841, Molecular Probes/MoBiTec) 4 weeks after ONI and 2–3 days prior to histological dissection (supplementary material Fig. S1). Atraumatic intravitreal injections were performed with a 5- $\mu$ l Hamilton syringe connected to a 34 G needle in the infero-temporal circumference  $\sim$ 1 mm distal of the corneo-scleral circumference, thereby sparing scleral vessels. To monitor needle insertion and liquid inoculation and to avoid lens puncture, microinjections were accomplished under a binocular microscope (Zeiss, Jena, Germany).

### Immunohistochemistry and immunocytochemistry

NF- $\kappa$ B *RelA* expression was evaluated using antibodies against *RelA* (polyclonal C-20, 1:500; Santa Cruz, Heidelberg, Germany), phosphorylated *RelA* (monoclonal pSer-536 clone 93H1, 1:200–1:500; Cell Signaling, Frankfurt, Germany) and NLS-*RelA* (monoclonal MAB 3026 clone 12H11, 1:250; Millipore, Darmstadt, Germany). Axonal degeneration and regeneration were assessed by co-staining with antibodies against phosphorylated neurofilaments (SMI-31, monoclonal, 1:500; Sternberger Monoclonals, Lutherville, MD), MAP-2 (monoclonal, 1:500; Chemicon) and GAP-43 (polyclonal, 1:250; Chemicon). For cellular colocalization, antibodies against markers of RGCs (TUJ-1, monoclonal, 1:250; Covance, Munich, Germany), Müller glia (CRALBP, monoclonal, 1:250; Abcam, Cambridge, MA) and GLAST, polyclonal, 1:250; Santa Cruz), astrocytes (GFAP, polyclonal, 1:500; Dako,

Hamburg, Germany) and ODCs (CAII, polyclonal, 1:500; Santa Cruz) were used. The expression of the reporters EGFP and  $\beta$ -galactosidase were assessed with antibodies against GFP (polyclonal, 1:100, Santa Cruz) and  $\beta$ -gal (polyclonal, 1:500; Chemicon). Inflammatory responses (not shown) were evaluated with antibodies against CD11b (monoclonal, 1:500; Serotec, Düsseldorf, Germany), Iba1 (polyclonal, 1:250; Wako Chemicals, Richmond, VA) and F4/80 (polyclonal, 1:500; Dianova, Hamburg, Germany). Glial scar formation was investigated by using antibodies against neurocan (monoclonal, 1:250; Abcam) and GFAP (polyclonal, 1:500; Dako). Cdh1 and Id2 in cultured hippocampal neurons were detected using antibodies against Fizzy-related (monoclonal, 1:500; Novus Biologicals, Cambridge, UK) and polyclonal, 1:500; Invitrogen, Darmstadt, Germany) and Id2 (polyclonal, 1:500; Santa Cruz). Suitable secondary antibodies were used to visualize primary antibody binding. Photomicrographs were captured with Zeiss AxioVision 2 (Zeiss, Jena, Germany) and AxioImager microscopes (software AxioVision 4.8; Zeiss).

### X-gal and Fluoro Jade B staining

Optic nerves and retinae of  *$\kappa$ B-lacZ* reporter mice were fixed in 2% paraformaldehyde (PFA), 0.2% glutaraldehyde in PBS (4°C) for 10 min, washed and incubated in X-gal staining solution (Roche, Mannheim, Germany) for 24 h at 37°C. Samples of liver and thymus were taken as positive controls.

Longitudinal optic nerve sections were immersed in 1% sodium hydroxide in 80% ethanol for 5 min, followed by incubation in 70% ethanol and distilled water for 2 min. For background suppression, slides were incubated in 0.06% potassium permanganate for 10 min. The staining solution was prepared from a 0.01% stock of Fluoro Jade B (Chemicon) in 0.1% acetic acid and freshly used at a final concentration of 0.0004%. After a 20-min incubation, slides were rinsed in distilled water, dried at 50°C, cleared with xylene and covered with ImmuMount<sup>TM</sup> (Shandon, Pittsburgh, PA).

### Electron microscopy

Animals were transcardially perfused with ice-cold PBS and freshly prepared fixative containing 1% PFA, 3% glutaraldehyde, 0.5% acrylaldehyde and 0.05 M CaCl<sub>2</sub> in 0.1 M cacodylate buffer pH 7.3. Optic nerves were fixed at 4°C overnight and processed for ultrafine sectioning on an EMTP tissue processor (Leica, Wetzlar, Germany). Specimens were rinsed six times (15 min/rinse) in 0.1 M cacodylate buffer and postfixed in 1% osmium and 1% potassium hexacyanoferrate II in 0.1 M cacodylate buffer at 4°C for 1 h. Following rinsing in cacodylate buffer and distilled water, optic nerves were dehydrated in acetone (30%, 50%, 70%, 90% and 95% solutions; 30 min at each step; Merck, Darmstadt, Germany), then twice in 100% acetone (45 min each). Samples were transferred to acetone-resin (EPON) composites and embedded for polymerization. Ultrathin sections of 50-nm thickness were cut with Reichert Ultracut S knives (Leica) and 35° diamond blades (Diatome, Hatfield, PA). Ultramicrographs were captured by a transmission electron microscope (JEM 1400, Jeol, Ehing, Germany) under 80 kV using a CCD camera (Orius SC 1000, Gatan Munich, Germany).

### Quantification of RGCs, ODCs and axonal regeneration

At 4 weeks after ONI, retinae were fixed in 4% PFA in PBS pH 7.4, flattened on glass slides and subjected to immunohistochemical procedures using the RGC marker TUJ-1. RGC densities were assessed at 3–4/6 radial eccentricity under a fluorescence microscope (AxioImager, Zeiss). Fluorescence microscopy was also used to quantify ODCs in 10- $\mu$ m longitudinal cryosections of the naïve optic nerve after labeling with anti-CAII antibodies.

Serial quantification of growth responses in anterogradely traced optic nerves was performed using the AutMess imaging program (Zeiss) supplemented by the AxioVision LE module under a 40 $\times$  objective (AxioImager, Zeiss). Because the undiluted CTX tracer displays defined invariable signal intensity, the threshold for signal detection was similar for all groups and specimens. Fields of regeneration (regions of interest, ROIs) were automatically identified and summed to define the total

regenerative area in each slice. The total regenerative area of each optic nerve was determined by summing the ROIs of all the slices.

### Immunoblotting

Lysates of retinae and optic nerves were subjected to SDS-PAGE and processed for immunoblotting according to standard protocols. Antibodies against the following proteins were used: RelA (polyclonal C-20, 1:1000; Santa Cruz), phosphorylated RelA (monoclonal pSer536 clone 93H1, 1:1000; Cell Signaling), NLS-RelA (monoclonal MAB 3026 clone 12H11, 1:500; Millipore), MBP (polyclonal, 1:200; Millipore), Id2 (polyclonal, 1:500; Santa Cruz), Cdh1 (Fizzy-related, monoclonal, 1:500; Novus Biologicals) and EM11 (monoclonal, 1:500; Invitrogen). Antibody against  $\beta$ -actin (polyclonal, 1:10,000; Abcam) was applied as loading control. Experiments were repeated at least three times for three different specimens.

### In vitro experiments

For immunocytochemistry on primary neurons, cultures of embryonic day (E)16 hippocampi of *RelA<sup>CNSKO</sup>* and *RelA<sup>fllox</sup>* mice were stained with antibodies against SMI-31, Cdh1 and Id2 and counterstained with DAPI. Our protocol for embryonic genotype-specific neuronal cultures from transgenic mice is available on request. The intranuclear-to-cytoplasmic switch of the signals was semi-quantitatively assessed using a Zeiss AxioImager microscope and AxioVision imaging software (Zeiss).

OLN-93 cells were grown as monolayers in sterile DMEM supplemented with 10% fetal bovine serum for 5 days at 37°C, under 5% CO<sub>2</sub> and with controlled humidity. To induce differentiation, the serum concentration was reduced to 0.5% for 5 days. Immunostaining with antibodies against NLS-RelA or RelA (C-20) (see above) was performed 30 min after treatment with TNF (20 ng/ml; Sigma, Germany) or PBS.

### Optometric measurement

Visual acuity and contrast sensitivity were investigated, making use of the optokinetic reflex in a virtual-reality optomotor device. Freely moving animals were subjected to moving sine wave gratings of various spatial frequencies and contrasts. Gratings were varied up to the detection threshold of reflexive head tilting (Prusky et al., 2004). Animals in the knockout and control groups were analyzed at identical time-points within the circadian rhythm.

### Statistical analysis

Statistical analyses were performed using the Student's *t*-test for single comparisons, followed by post-hoc test calculation. Data are presented as the mean  $\pm$  s.e.m. For each experiment, individual *n* numbers are given separately. Results reaching  $P \leq 0.05$  were considered to be statistically significant (\* $P < 0.05$ , \*\* $P < 0.01$ , \*\*\* $P < 0.001$ , # $P > 0.05$ ).

### Acknowledgements

We appreciate the provision of inducible GLAST-Cre mice by Frank W. Pfrieger (Institute of Cellular and Integrative Neuroscience, Strasbourg, France) and the OLN-93 cell line by Christiane Richter-Landsberg (Carl von Ossietzky University, Oldenburg, Germany). We thank Svetlana Tausch (Hans Berger Department of Neurology, Jena, Germany) for technical assistance and Maik Baldauf (Leibniz Institute for Age Research, Jena, Germany) for histological assistance. We are grateful to Katrin Buder (Leibniz Institute for Age Research) for the support on ELMI and Silvio Schmidt (Hans Berger Department of Neurology) and Ines Krumbein (Institute of Diagnostic and Interventional Radiology, Jena, Germany) for MRI advice.

### Competing interests

The authors declare no competing interests.

### Author contributions

R.H. and A.K. organized the study and prepared the manuscript. K.-H.H. developed the MEMRI protocol. K.K. and K.-F.S. conducted the functional animal tasks. C.E. performed cell culture experiments. K.-A.N. provided the Cre line for the creation of ODC-specific mouse mutants. F.W., O.W.W., S.L. and J.R.R. supervised and financed the study and helped with data interpretation.

### Funding

R.H. is supported by the VELUX Foundation (Switzerland; grant number 806); A.K. was supported by the Interdisziplinäres Zentrum für Klinische Forschung (IZKF), Jena, and the Oppenheim-Foundation/Novartis.

### Supplementary material

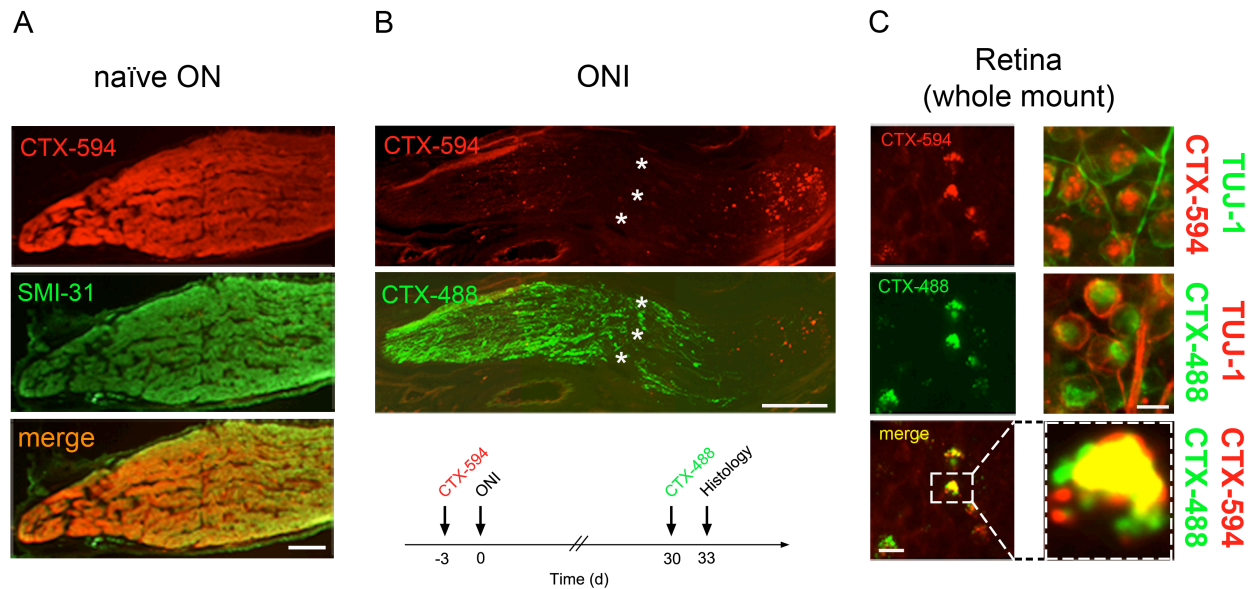
Supplementary material available online at <http://jcs.biologists.org/lookup/suppl/doi:10.1242/jcs.140731/-DC1>

### References

- Algül, H., Treiber, M., Lesina, M., Nakhai, H., Saur, D., Geisler, F., Pfeifer, A., Paxian, S. and Schmid, R. M. (2007). Pancreas-specific RelA/p65 truncation increases susceptibility of acini to inflammation-associated cell death following cerulein pancreatitis. *J. Clin. Invest.* **117**, 1490–1501.
- Brambilla, R., Bracchi-Ricard, V., Hu, W. H., Frydel, B., Bramwell, A., Karmally, S., Green, E. J. and Bethea, J. R. (2005). Inhibition of astroglial nuclear factor kappaB reduces inflammation and improves functional recovery after spinal cord injury. *J. Exp. Med.* **202**, 145–156.
- Brambilla, R., Hurtado, A., Persaud, T., Esham, K., Pearse, D. D., Oudega, M. and Bethea, J. R. (2009). Transgenic inhibition of astroglial NF-kappa B leads to increased axonal sparing and sprouting following spinal cord injury. *J. Neurochem.* **110**, 765–778.
- Chen, M. S., Huber, A. B., van der Haar, M. E., Frank, M., Schnell, L., Spillmann, A. A., Christ, F. and Schwab, M. E. (2000). Nogo-A is a myelin-associated neurite outgrowth inhibitor and an antigen for monoclonal antibody IN-1. *Nature* **403**, 434–439.
- Choi, J.-S., Sungjoo, K. Y. and Joo, C.-K. (1998). NF- $\kappa$  B activation following optic nerve transection. *Korean J. Ophthalmol.* **12**, 19–24.
- Chua, H. L., Bhat-Nakshatri, P., Clare, S. E., Morimiya, A., Badve, S. and Nakshatri, H. (2007). NF-kappaB represses E-cadherin expression and enhances epithelial to mesenchymal transition of mammary epithelial cells: potential involvement of ZEB-1 and ZEB-2. *Oncogene* **26**, 711–724.
- De Lima, S., Koriyama, Y., Kurimoto, T., Oliveira, J. T., Yin, Y., Li, Y., Gilbert, H. Y., Fagiolini, M., Martinez, A. M. and Benowitz, L. (2012). Full-length axon regeneration in the adult mouse optic nerve and partial recovery of simple visual behaviors. *Proc. Natl. Acad. Sci. USA* **109**, 9149–9154.
- Emmanouil, M., Taoufik, E., Tseveleki, V., Vamvakas, S. S., Tselios, T., Karin, M., Lassmann, H. and Probert, L. (2009). Neuronal I kappa B kinase beta protects mice from autoimmune encephalomyelitis by mediating neuroprotective and immunosuppressive effects in the central nervous system. *J. Immunol.* **183**, 7877–7889.
- Fischer, S., Engelmann, C., Herrmann, K.-H., Reichenbach, J. R., Witte, O. W., Weih, F., Kretz, A. and Haenold, R. (2014). In vivo imaging of optic nerve fiber integrity by contrast-enhanced MRI in mice. *JOVE*. (in press)
- Gavaldà, N., Gutierrez, H. and Davies, A. M. (2009). Developmental switch in NF-kappaB signalling required for neurite growth. *Development* **136**, 3405–3412.
- Gutierrez, H. and Davies, A. M. (2011). Regulation of neural process growth, elaboration and structural plasticity by NF- $\kappa$ B. *Trends Neurosci.* **34**, 316–325.
- Gutierrez, H., O'Keefe, G. W., Gavaldà, N., Gallagher, D. and Davies, A. M. (2008). Nuclear factor kappa B signaling either stimulates or inhibits neurite growth depending on the phosphorylation status of p65/RelA. *J. Neurosci.* **28**, 8246–8256.
- Haenold, R., Herrmann, K.-H., Schmidt, S., Reichenbach, J. R., Schmidt, K.-F., Löwel, S., Witte, O. W., Weih, F. and Kretz, A. (2012). Magnetic resonance imaging of the mouse visual pathway for in vivo studies of degeneration and regeneration in the CNS. *Neuroimage* **59**, 363–376.
- Herrero-Mendez, A., Almeida, A., Fernández, E., Maestre, C., Moncada, S. and Bolaños, J. P. (2009). The bioenergetic and antioxidant status of neurons is controlled by continuous degradation of a key glycolytic enzyme by APC/C-Cdh1. *Nat. Cell Biol.* **11**, 747–752.
- Huang, C. J., Nazarian, R., Lee, J., Zhao, P. M., Espinosa-Jeffrey, A. and de Vellis, J. (2002). Tumor necrosis factor modulates transcription of myelin basic protein gene through nuclear factor kappa B in a human oligodendrogloma cell line. *Int. J. Dev. Neurosci.* **20**, 289–296.
- Huynh, M. A., Stegmüller, J., Litterman, N. and Bonni, A. (2009). Regulation of Cdh1-APC function in axon growth by Cdh1 phosphorylation. *J. Neurosci.* **29**, 4322–4327.
- Imielski, Y., Schwamborn, J. C., Lüningschrör, P., Heimann, P., Holzberg, M., Werner, H., Leske, O., Püschel, A. W., Memet, S., Heumann, R. et al. (2012). Regrowing the adult brain: NF- $\kappa$ B controls functional circuit formation and tissue homeostasis in the dentate gyrus. *PLoS ONE* **7**, e30838.
- Inta, I., Paxian, S., Maegele, I., Zhang, W., Pizzi, M., Spano, P., Sarnico, I., Muhammad, S., Herrmann, O., Inta, D. et al. (2006). Bim and Noxa are candidates to mediate the deleterious effect of the NF- $\kappa$  B subunit RelA in cerebral ischemia. *J. Neurosci.* **26**, 12896–12903.
- Kaltschmidt, B. and Kaltschmidt, C. (2009). NF-kappaB in the nervous system. *Cold Spring Harb. Perspect. Biol.* **1**, a001271.
- Katoh, M. and Katoh, M. (2009). Integrative genomic analyses of ZEB2: Transcriptional regulation of ZEB2 based on SMADs, ETS1, HIF1alpha, POU/OCT, and NF-kappaB. *Int. J. Oncol.* **34**, 1737–1742.
- Kim, N. S., Kim, H. J., Koo, B. K., Kwon, M. C., Kim, Y. W., Cho, Y., Yokota, Y., Penninger, J. M. and Kong, Y. Y. (2006). Receptor activator of NF-kappaB

- ligand regulates the proliferation of mammary epithelial cells via Id2. *Mol. Cell Biol.* **26**, 1002-1013.
- Konishi, Y., Stegmüller, J., Matsuda, T., Bonni, S. and Bonni, A. (2004). Cdh1-APC controls axonal growth and patterning in the mammalian brain. *Science* **303**, 1026-1030.
- Kretz, A., Herrmann, K. H., Fischer, S., Engelmann, C., Witte, O. W., Reichenbach, J. R., Weih, F. and Haenold, R. (2013). Dysfunctional NF- $\kappa$ B and brain myelin formation. *Eur. J. Hum. Genet.* **22**, 724-725.
- Lang, H., Schulte, B. A., Zhou, D., Smythe, N., Spicer, S. S. and Schmiedt, R. A. (2006). Nuclear factor kappaB deficiency is associated with auditory nerve degeneration and increased noise-induced hearing loss. *J. Neurosci.* **26**, 3541-3550.
- Lappe-Siefke, C., Goebbels, S., Gravel, M., Nicksch, E., Lee, J., Braun, P. E., Griffiths, I. R. and Nave, K.-A. (2003). Disruption of Cnp1 uncouples oligodendroglial functions in axonal support and myelination. *Nat. Genet.* **33**, 366-374.
- Lasorella, A., Stegmüller, J., Guardavaccaro, D., Liu, G., Carro, M. S., Rothschild, G., de la Torre-Ubieta, L., Pagano, M., Bonni, A. and Iavarone, A. (2006). Degradation of Id2 by the anaphase-promoting complex couples cell cycle exit and axonal growth. *Nature* **442**, 471-474.
- Li, J., Lu, Z., Li, W. L., Yu, S. P. and Wei, L. (2008). Cell death and proliferation in NF-kappaB p50 knockout mouse after cerebral ischemia. *Brain Res.* **1230**, 281-289.
- Lu, Z. Y., Yu, S. P., Wei, J. F. and Wei, L. (2006). Age-related neural degeneration in nuclear-factor kappaB p50 knockout mice. *Neuroscience* **139**, 965-978.
- Meffert, M. K., Chang, J. M., Wiltgen, B. J., Fanselow, M. S. and Baltimore, D. (2003). NF-kappa B functions in synaptic signaling and behavior. *Nat. Neurosci.* **6**, 1072-1078.
- Misantone, L. J., Gershenbaum, M. and Murray, M. (1984). Viability of retinal ganglion cells after optic nerve crush in adult rats. *J. Neurocytol.* **13**, 449-465.
- Prusky, G. T., Alam, N. M., Beekman, S. and Douglas, R. M. (2004). Rapid quantification of adult and developing mouse spatial vision using a virtual optomotor system. *Invest. Ophthalmol. Vis. Sci.* **45**, 4611-4616.
- Raasch, J., Zeller, N., van Loo, G., Merkler, D., Mildner, A., Erny, D., Knobloch, K. P., Bethea, J. R., Waisman, A., Knust, M. et al. (2011). IkkappaB kinase 2 determines oligodendrocyte loss by non-cell-autonomous activation of NF-kappaB in the central nervous system. *Brain* **134**, 1184-1198.
- Richter-Landsberg, C. and Heinrich, M. (1996). OLN-93: a new permanent oligodendroglia cell line derived from primary rat brain glial cultures. *J. Neurosci. Res.* **45**, 161-173.
- Schmidt-Ullrich, R., Mémet, S., Lilienbaum, A., Feuillard, J., Raphaël, M. and Israel, A. (1996). NF-kappaB activity in transgenic mice: developmental regulation and tissue specificity. *Development* **122**, 2117-2128.
- Sha, W. C., Liou, H. C., Tuomanen, E. I. and Baltimore, D. (1995). Targeted disruption of the p50 subunit of NF- $\kappa$ B leads to multifocal defects in immune responses. *Cell* **80**, 321-330.
- Slezak, M., Göritz, C., Niemiec, A., Frisé, J., Chambon, P., Metzger, D. and Pfrieger, F. W. (2007). Transgenic mice for conditional gene manipulation in astroglial cells. *Glia* **55**, 1565-1576.
- Soriano, P. (1999). Generalized lacZ expression with the ROSA26 Cre reporter strain. *Nat. Genet.* **21**, 70-71.
- Srinivas, S., Watanabe, T., Lin, C. S., William, C. M., Tanabe, Y., Jessell, T. M. and Costantini, F. (2001). Cre reporter strains produced by targeted insertion of EYFP and ECFP into the ROSA26 locus. *BMC Dev. Biol.* **1**, 4.
- Takahashi, Y., Katai, N., Murata, T., Taniguchi, S. I. and Hayashi, T. (2007). Development of spontaneous optic neuropathy in NF- $\kappa$ Bp50-deficient mice: requirement for NF- $\kappa$ Bp50 in ganglion cell survival. *Neuropathol. Appl. Neurobiol.* **33**, 692-705.
- Yu, P., Zhang, Y. P., Shields, L. B., Zheng, Y., Hu, X., Hill, R., Howard, R., Gu, Z., Burke, D. A., Whittemore, S. R. et al. (2011). Inhibitor of DNA binding 2 promotes sensory axonal growth after SCI. *Exp. Neurol.* **231**, 38-44.
- Zhang, W., Potrovita, I., Tarabin, V., Herrmann, O., Beer, V., Weih, F., Schneider, A. and Schwaneinger, M. (2005). Neuronal activation of NF-kappaB contributes to cell death in cerebral ischemia. *J. Cereb. Blood Flow Metab.* **25**, 30-40.

## Supplemental Information



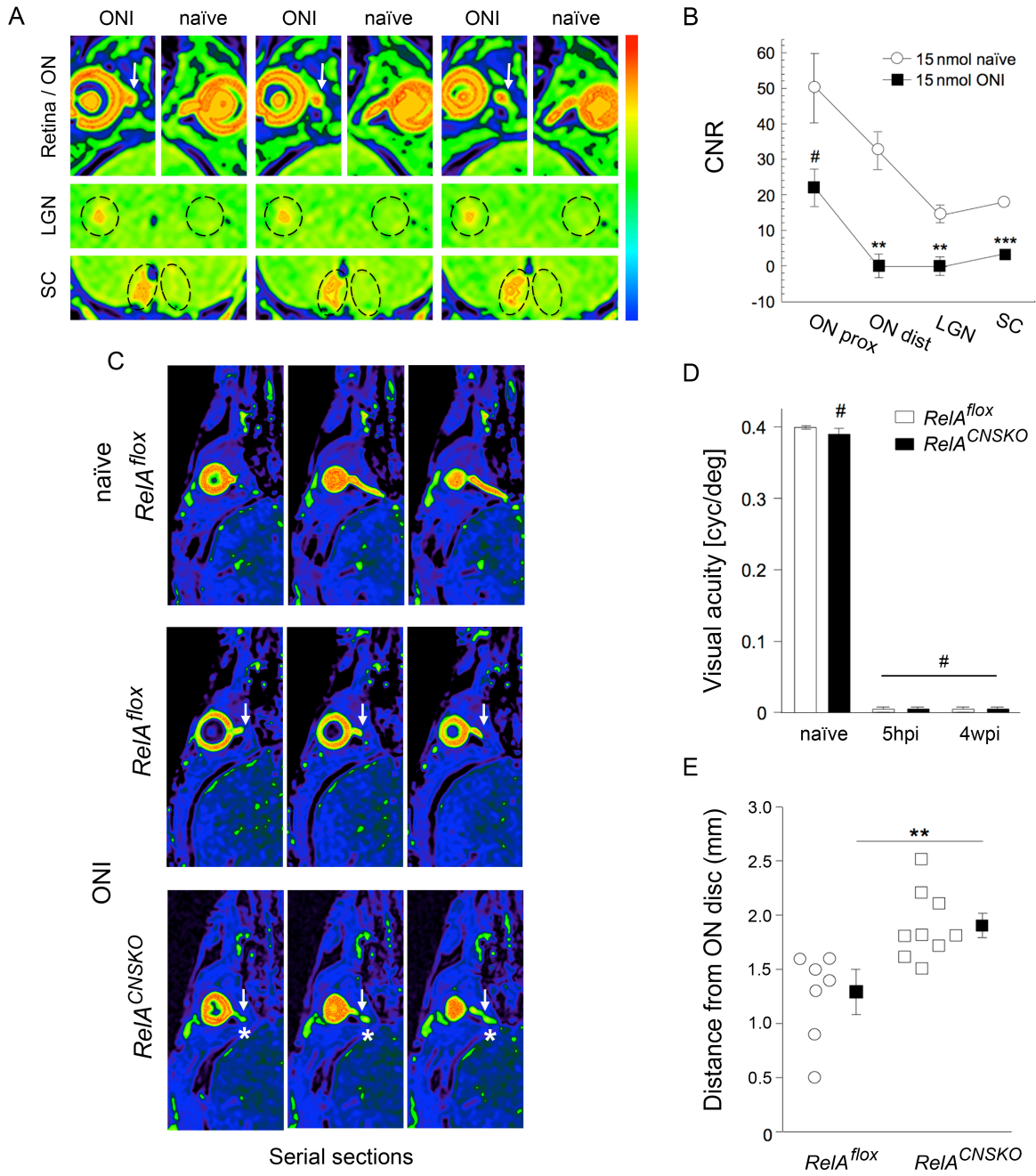
Suppl. Figure 1

**Suppl. Figure 1. Tracer-based axonal de- versus regeneration for growth studies after ONI.**

(A) In the naïve state, intravitreal applied CTX-594 (red) becomes anterogradely transported along the optic nerve (ON) and co-localizes with the axonal marker SMI-31. Scale bar, 150  $\mu\text{m}$ .

(B) Disappearance of CTX-594 applied prior to ONI indicated Wallerian degeneration of injured RGC axons. Complementary CTX-488 (green) introduced at the end of the growth period solely labeled *de novo* generated axons (asterisks, lesion site). Scale bar, 200  $\mu\text{m}$ . Bottom: Scheme on tracer application 3 days before and 4 weeks after ONI.

(C) Origin of regenerating fibers from surviving, but initially deafferented RGC was verified by uptake of both markers into individual cell somata (left panel). Note that intracellular precipitated and granular CTX does not label the cell membrane (dotted box: magnification of merge image). Scale bar, 30  $\mu\text{m}$ . Right panel: Incorporation of complementary Alexa-594 and Alexa-488 CTX conjugates into naïve and post-lesional RGCs was proven by TUJ-1 co-staining. Scale bar, 25  $\mu\text{m}$ .



Suppl. Figure 2

**Suppl. Figure 2. Serial MEMRI for mapping viability, de- and regeneration of optic nerve axons.** (A) Imaging of the visual projection by MEMRI delineated tracer propagation along the intact right optic nerve (ON), contralateral lateral geniculate nucleus (LGN) and superior colliculus (SC), whereas injury of the left optic nerve (arrows in top panel) resulted in complete signal extinction caudal to the injury site (empty dashed circles; n=5). Scale bar: warm colors indicate high signal intensity. (B) Quantitative analysis confirmed a decline of CNR to background levels caudal to the lesion site (n=5). (C) Four weeks after ONI, tracer propagation was partially restituted beyond the lesion site (arrows) in *RelA<sup>CNSKO</sup>* mice (bottom panel; asterisks), but not in controls (middle panel) (n=9). Since manganese transport is an active process that requires calcium exchange, positive CNR reflects fiber vitality. (D) Measurement of visual acuity indicated complete blindness of all animals immediately after ONI that persisted for more than 4 weeks and thus excluded a transient conduction block (n=5). (E) Retro-bulbar distances of axonal manganese transport in *RelA<sup>CNSKO</sup>* mice were significantly increased as compared to controls (n=9 for *RelA<sup>CNSKO</sup>*; n=7 for *RelA<sup>fllox</sup>*). hpi, hours post injury; wpi, weeks post injury.